Quaternary Science Reviews 308 (2023) 108082

Contents lists available at ScienceDirect

Quaternary Science Reviews

journal homepage: www.elsevier.com/locate/quascirev

Tracking sediment delivery to central Baffin Bay during the past 40 kyrs: Insights from a multiproxy approach and new age model

Emma Ownsworth [a, *], David Selby [a], Jeremy Lloyd [b], Paul Knutz [c], Sönke Szidat [d], John Andrews [e], Colm Ó Cofaigh [b]

[a] Department of Earth Sciences, Durham University, Durham, DH1 3LE, UK
[b] Department of Geography, Durham University, Durham, DH1 3LE, UK
[c] Geological Survey of Denmark and Greenland (GEUS), 1350, Copenhagen K, Denmark
[d] Department of Chemistry, Biochemistry and Pharmaceutical Sciences & Oeschger Centre for Climate Change Research, University of Bern, CH-3012, Bern, Switzerland
[e] INSTAAR and Department of Geological Sciences, University of Colorado, Boulder, CO, 80309, USA

ARTICLE INFO

Article history:
Received 1 December 2022
Received in revised form
4 April 2023
Accepted 5 April 2023
Available online 19 April 2023

Handling Editor: A. Voelker

Keywords:
Quaternary
Baffin Bay
Greenland ice sheet
Laurentide ice sheet
Innuitian ice sheet
Paleoclimate
Radiocarbon
Osmium isotopes
Detrital carbonate

ABSTRACT

Reconstructing former ice sheet history and glaciogenic sediment fluxes surrounding Baffin Bay during and since the Last Glacial Maximum (LGM) is a major scientific challenge. Here, a new multi-proxy analysis of sediments from a central Baffin Bay (BB) sediment core reveals two dominant sediment/discharge sources: 1) a detrital carbonate (BBDC; dolomite-rich) source that represents increased discharge from the NE Laurentide Ice Sheet (LIS) and southern Innuitian Ice Sheet (IIS), and 2) a radiogenic, felsic provenance likely from a west Greenland Ice Sheet (GIS) source, although a contribution from the Baffin Island LIS cannot be ruled out. By utilising a new method for radiocarbon calibration in high latitude polar environments we provide updated age constraints on BBDC1 (14.1–13 cal ka BP) and BBDC0 (12.0–10.9 cal ka BP). This coupled with our sediment analysis shows the BBDC layers to be coincident with the Bølling-Allerød (BBDC1) and the recovery from the Younger Dryas (BBDC0). The timing of BBDC1 also further supports the theory of an ice shelf covering northern Baffin Bay from the LGM and during initial deglaciation.

1. Introduction

The geological similarities of Baffin Island and Greenland has hampered sediment provenance identification of Holocene and Late Pleistocene-aged sediments of Baffin Bay. Although some progress has been made, it has proven challenging and hence makes understanding the temporal relationships of ice sheet dynamics between the LIS, IIS, and GIS during the last glacial cycle difficult (Aksu and Piper, 1979; Andrews, 2019; Andrews et al., 2014, 2018; Andrews and Eberl, 2011; Briner et al., 2006; Harrison et al., 2011; Jackson et al., 2017; Jennings et al., 2018; Knutz et al., 2022; Ó Cofaigh et al., 2013a, 2013b; Simon et al., 2014; St-Onge et al., 2009).

The majority of chronologies and correlations of Holocene and Late Pleistocene-aged sediments of Baffin Bay rely on layers of carbonate-rich sediments, termed Baffin Bay Detrital Carbonate (BBDC) layers that were deposited in response to increased ice discharge, mainly through the Lancaster Sound ice stream, from the NE LIS and southern IIS that covered areas of Paleozoic-age carbonate-rich rocks during the MIS2 to MIS4 (Fig. 1) (Andrews, 1987; Andrews et al., 1998; Andrews and Eberl, 2011; Dalton et al., 2020; Kelleher et al., 2022; Simon et al., 2014). Ice rafted debris (IRD) from the LIS and the GIS, which covered areas of mainly Archean to Paleoproterozoic granites, gneisses, and metasedimentary units may also have contributed to the BBDC layers (Aksu and Piper, 1987; Harrison et al., 2011; Henriksen and Higgins, 2009; Simon et al., 2012, 2014). Detailed lithostratigraphic analysis on the Baffin Island shelf have shown that changes in the lithofacies represent changes in the transport and provenance of sediments into the area

* Corresponding author.
E-mail address: e.m.ownsworth@durham.ac.uk (E. Ownsworth).

https://doi.org/10.1016/j.quascirev.2023.108082

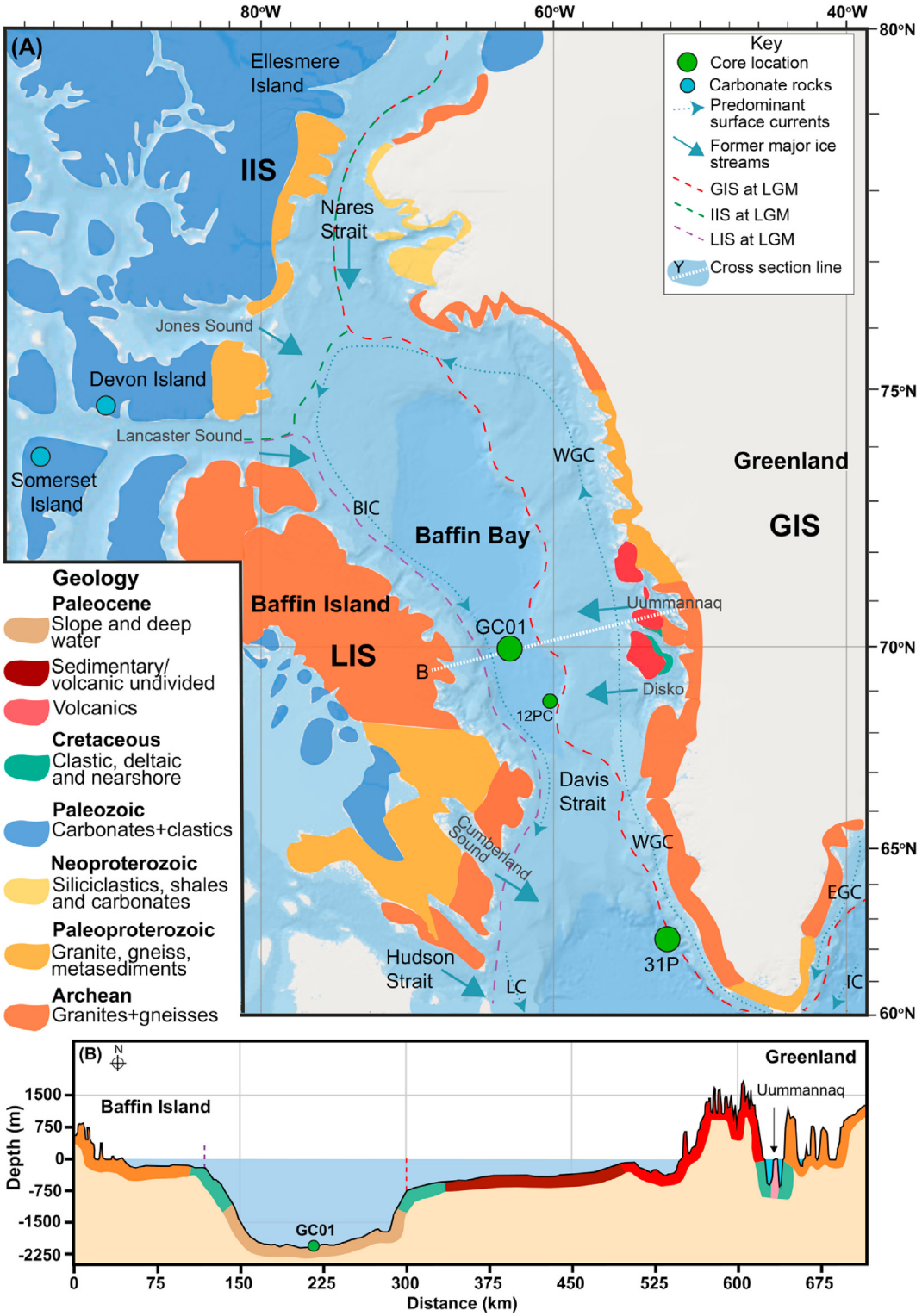

Fig. 1. Baffin Bay map, cross section, and geology. (**A**) Baffin Bay and surrounding ice sheets with estimated Last Glacial Maximum (LGM) ice margins and the simplified surrounding geology. Core 12 PC is core HU2008029−12 PC (Jennings et al., 2018). Base map from ArcGIS. Geology, circulation patterns and ice sheet extents extracted from (Harrison et al., 2011) and (Simon et al., 2014) and references therein (England et al., 2006; Gregersen et al., 2016; Knutz et al., 2022; Ó Cofaigh et al., 2013b; Tang et al., 2004). GIS = Greenland Ice Sheet, IIS = Innuitian Ice Sheet, LIS = Laurentide Ice Sheet. On west Greenland the geology includes Archean gneisses and granites of the North Atlantic Craton and Aasiaat Domain, and Archean to Paleoproterozoic metasediments, gneisses and granites of the Rae Craton (Gregersen et al., 2016; Harrison et al., 2011; Henriksen and Higgins, 2009; Knutz et al., 2022; Simon et al., 2012, 2014). Similarly, east Baffin Island comprises metamorphosed clastics, granites, gneisses and volcanics of the Rae Craton, Foxe Fold Belt, and Cumberland Batholith. The central abyssal plain mainly comprises fan-delta sandstones and interbedded mudstones (Harrison et al., 2011). Paleozoic carbonate and clastic outcrops in N/NW of Baffin Bay continue through the Canadian Arctic Channels, seafloor and smaller islands through Lancaster and Jones Sound. Paleocene volcanic outcrops include basalts and picrites (Harrison et al., 2011; Henriksen and Higgins, 2009; Simon et al., 2012, 2014). Dominant, present-day anti-clockwise circulation results from the Irminger Current (IC) and East Greenland Current (EGC) combining into the West Greenland Current (WGC) flowing through the Davis Strait into Baffin Bay where in the north it mixes with colder Arctic waters becoming the Baffin Island Current (BIC) and heading back south, eventually flowing back out the Davis Strait into the Labrador Current (LC), with some recirculated back towards

linked to the movements of the major ice sheets surrounding Baffin Bay over the last glacial cycle (Andrews et al., 2020; Jenner et al., 2018).

To provide an improved understanding of transport and provenance of sediments, and glacial movements of the three major ice sheets that surrounded Baffin Bay over the last ~40 kyrs, we present a multi-proxy study that includes the first osmium (Os) isotope ($^{187}Os/^{188}Os$) record of Baffin Bay. Osmium isotope data of sediments has been applied to understand the interplay between silicate weathering, and palaeoceanographic processes during the Holocene, Pleistocene glacial-interglacial cycles, Oligocene, Silurian, Late Ordovician and Neoproterozoic glacial events (Burton et al., 2010; Dalai et al., 2005, 2006; Dalai and Ravizza, 2006; Finlay et al., 2010; Oxburgh, 1998; Oxburgh et al., 2007; Paquay et al., 2009; Paquay and Ravizza, 2012; Peucker-Ehrenbrink and Ravizza, 2000; Rooney et al., 2014, 2016; Sproson et al., 2022; Williams and Turekian, 2004). The hydrogenous $^{187}Os/^{188}Os$ composition of organic-rich sediment units is used to establish a high-resolution record of the water column at the time of deposition. The $^{187}Os/^{188}Os$ of present day seawater ($^{187}Os/^{188}Os$ of ~1.0) is relatively similar across the Earth's oceans and reflects a balance of radiogenic Os from continental inputs ($^{187}Os/^{188}Os$ average = ~1.4, but old crystalline rocks can be much higher, >2) (Peucker-Ehrenbrink and Jahn, 2001) and unradiogenic Os from mantle/hydrothermal inputs ($^{187}Os/^{188}Os$ = ~0.12) (Peucker-Ehrenbrink and Ravizza, 2000). Specific to this study, $^{187}Os/^{188}Os$ data from Holocene-age sediments in the Disko Bugt-Uummannaq region demonstrate the ability to identify shifts in the flux of glacially eroded material from the GIS and thus track ice sheet advance and retreat patterns which broadly correlate with the known deglacial history of the Jakobshavn Isbræ ice stream (Rooney et al., 2016). Moreover, the application of Os isotope stratigraphy revealed greater detail of the ice sheet calving history of Jakobshavn Isbrae than previously recorded by the biostratigraphy and that Os isotope data has the potential to better decode the dynamic behaviour of ice sheets at millennial timescales. Coupled with the osmium isotope data, major, trace, and rare element data can be a useful sediment provenance discriminator (Bhatia and Crook, 1986; Taylor and McLennan, 1985).

Here we aim to improve our understanding of the sediment flux contributions from the GIS, IIS and LIS and its relation to climate and ocean forcing scenarios (Jennings et al., 2014, 2017; Sheldon et al., 2016; Simon et al., 2014). To achieve this, we investigate a central Baffin Bay gravity core (JR175-GC01 – referenced as GC01) presenting high-resolution, multi-proxy data including core sedimentology coupled with microfossil and geochemical data (XRF, XRD and REE, and osmium isotopes) together with new radiocarbon dates to provide a Bayesian age model, and additional data from a core south of Davis Strait near the entrance to Baffin Bay (DA04-31 P, referenced as 31 P) (Knutz et al., 2011). We also utilise a new method for calibration of radiocarbon dates from high latitude polar locations, trying to address longstanding issues with uncertainty in the reservoir corrections in these areas (Heaton et al., 2020, 2022, 2023; Reimer et al., 2013, 2020; Stuiver et al., 2020), and in doing so aim to be able to provide updated age constraints for BBDC1 and BBDC0.

2. Regional setting and glacial history

Baffin Bay is a narrow (max width = 650 km) ocean basin connected to the Atlantic Ocean through the Davis Strait and Labrador Sea with a number of interlinking present-day currents creating an anti-clockwise circulation in the bay (Fig. 1a) (Aksu and Piper, 1979; Andrews, 1987; Andrews et al., 1998, 2014; Simon et al., 2012; Tang et al., 2004). The central abyssal plain of Baffin Bay is ca. 2 km deep, shallowing towards the north and south and mainly comprising Neogene-aged sediments, fan-delta sandstones and interbedded mudstones (Aksu and Piper, 1979; Harrison et al., 2011; Li et al., 2011). The west Greenland continental shelf is relatively wide (135–200 km) and is bisected by a number of troughs leading to large trough mouth fans (Henriksen and Higgins, 2009; Knutz et al., 2019; Ó Cofaigh et al., 2013a, 2013b). On the western side of the bay, the Baffin Island shelf is narrower (25–50 km) with only minor trough mouth fan development (Fig. 1b) (Andrews et al., 2014; Li et al., 2011). Prior to the formation of Baffin Bay through rifting during the Cretaceous-Paleocene, Greenland and Baffin Island were joined and as a result share very similar geologies (Fig. 1) (Andrews et al., 2018; Harrison et al., 2011; Henriksen and Higgins, 2009; Knutz et al., 2022; St-Onge et al., 2009). The geology of both western Greenland and Baffin Island largely comprises Archean- and Paleoproterozoic-aged crystalline units, with some Paleocene-aged basalts and extensive Tertiary-aged volcanics on and around Disko Island, Uummannaq Fjord, Svartenhuk and also Cape Dyer on Baffin Island (Gregersen et al., 2016; Harrison et al., 2011; Henriksen and Higgins, 2009; Simon et al., 2014). In the northern and north-eastern regions of Baffin Bay, the crystalline basement is overlain by Paleozoic marine carbonate and clastic successions (Fig. 1a) (Gregersen et al., 2016; Harrison et al., 2011; Knutz et al., 2022; Simon et al., 2014).

The recent Quaternary sediments found within Baffin Bay largely originate from glacial erosion of the surrounding bedrock, transported into the basin by debris flows, meltwater plumes and icebergs (Aksu and Piper, 1979; Andrews and Eberl, 2011; Jenner et al., 2018; Ó Cofaigh et al., 2018). On the Greenland Shelf, the main sediment contribution is delivered by ice rafting and meltwater from the GIS (Andrews et al., 2018; Hogan et al., 2016; Hudson et al., 2014). On the Baffin Island shelf, transport of sediments is mainly through meltwater, with some fluvial inputs in the fjords (Andrews et al., 2018). Carbonate-rich sediments (predominantly dolomite) are mainly found in the north, north-west and down the central portion of Baffin Bay, with contributions thinning southwards along the bay (Andrews et al., 1998, 2018; Andrews and Eberl, 2011). Sediments enriched in basaltic rock detritus are found in localised ares of the Greenland Shelf near Disko Island (Andrews et al., 2018; Andrews and Eberl, 2011).

At the Last Glacial Maximum (LGM), Baffin Bay was surrounded by major ice sheets including the Greenland Ice Sheet (GIS) to the east, the Innuitian Ice Sheet (IIS) to the north, and the Laurentide Ice Sheet (LIS) to the west (Fig. 1) (Dyke et al., 2002; England et al., 2006; Jackson et al., 2017; Simon et al., 2012, 2014). However, the exact timings of when these ice sheets advanced and retreated from the continental shelves since the LGM remains uncertain (Andrews et al., 2018; Briner et al., 2006; Ó Cofaigh et al., 2013b). The ice sheets are generally thought to have reached their maximum extent during the LGM (Andrews et al., 2014; Briner et al., 2006, 2003; Clark et al., 2009; Dalton et al., 2022, 2020; Jenner et al., 2018; Ó Cofaigh et al., 2013b; Simon et al., 2014). The retreat of the GIS is gradual and diachronous along its margins, with the beginning of ice retreat around central-west Greenland varying between 17.1 and 16.2 cal ka BP depending on location (Jennings

Greenland (Aksu and Piper, 1979; Andrews, 1987; Jackson et al., 2017; Sheldon et al., 2016; Tang et al., 2004). (**B**) Cross section and simplified geology across Baffin Bay from Baffin Island to the west coast of Greenland. Line of the cross section is shown in part (**A**). Cross section profiles obtained from GoogleEarthPro. Geology modified from (Harrison et al., 2011).

et al., 2017). The timing of retreat of the LIS is less well constrained and in general is thought to have been underway by 16 cal ka BP (Brouard and Lajeunesse, 2017; Dalton et al., 2020), and with retreat of the Lancaster Sound ice stream underway by ~15.3 cal ka BP (Furze et al., 2018; Kelleher et al., 2022). Less constrained timings are, in part, due to slow sedimentation rates and poor preservation of biogenic carbonate during deglaciation into the Holocene, especially in deeper sedimentary records, as well as limited research on the LGM, which means that well-dated sedimentary records from within Baffin Bay are lacking (Andrews et al., 2018, 1998; Briner et al., 2006; Jackson et al., 2017; Jenner et al., 2018; Jennings et al., 2018; Ó Cofaigh et al., 2013b; Simon et al., 2012). The build up and retreat of the IIS is even less well studied, with build up as late as 19 cal ka BP, and with retreat after 11 cal ka BP (England et al., 2006).

3. Materials and methods

3.1. Cores and samples

Cores from two locations were analysed to provide different background information. The main core analysed using all the proxies listed below is from a central Baffin Bay position to decipher glacial related events (GC01). A second core, analysed only for its osmium isotope composition, is from the Davis Strait and is used to track ocean input into Baffin Bay and to represent an open ocean setting away from the immediate influence of grounded ice (31 P).

The 1.68 m gravity core (GC01) and associated boxcore (BC06) were collected during cruise JR175 of the RRS *James Clark Ross* (August–September 2009) at a latitude of 69°56′01″N and longitude of 63°03′4″W, and a water depth of 2034 m (Fig. 1; S1). Additional analysis of a second 8.78 m long piston core (31 P) is also presented (Fig. 1; S1), collected from a water depth of 2525 m at a latitude of 62°33′78″N and longitude of 54°22′W during a cruise of the R/V *Dana* in 2004 (Knutz et al., 2011). Twelve AMS radiocarbon dates on this core indicate *c*. 31 kyrs of sedimentation (Knutz et al., 2011).

A series of carbonate rock samples of the Paleozoic (Cambrian to Silurian) succession were also sampled and analysed for their $^{187}Os/^{188}Os$ signature to provide clearer detail on the potential source of the $^{187}Os/^{188}Os$ in the sediment cores (Fig. 1). These rocks were collected from north-west of Baffin Bay through Lancaster Sound on Somerset Island and Devon Island and are considered representative of the Paleozoic carbonate geologies of north and north-west Baffin Bay (Fig. 1; S1).

3.2. Particle size analysis (PSA)

Particle size analysis (PSA) was undertaken using ~0.5 g of sediment at 4 cm intervals through GC01 and following pre-established methods (Blott et al., 2004). In brief, organic matter and calcareous foraminifera were removed using hydrogen peroxide and hydrochloric acid, respectively. Sodium hexametaphosphate solution is added before analysis on a Coulter LS 13,320 laser diffraction PS analyser equipped with Polarisation Intensity Differential Scattering (PIDS). The data was then analysed using GRADISTAT (Blott and Pye, 2001).

3.3. X-ray imagery

A Geotek Vertical X-Ray CT system was used to produce 2D X-ray images of GC01 at $\leq$ 100 μm resolution. X-ray images were analysed at 2 cm intervals to identify clasts and sedimentary structures, and to count ice rafted debris (IRD clast >2 mm).

3.4. Total organic carbon

Total carbon (TC), total organic carbon (TOC) and total inorganic carbon (TIC) were measured in GC01 using an Analytik Jena Multi Elemental Analyser 4000. At ~4 cm intervals 20 g of sediment was freeze-dried, and ball milled. A 20–30 mg aliquot of every sample was used for the TC analysis, with 40–50 mg of sample used for the TIC run that was further treated with 40% orthophsphoric acid (to remove any organic component). Both were then combusted at 1000–1500 °C in the presence of O_2 and no catalyst, and the resulting gas was analysed by a Non-Dispersive Infrared (NDIR) detector. TOC was calculated as TOC = TC − TIC.

3.5. Foraminifera

Foraminiferal analysis (Feyling-Hanssen, 1964; Lloyd, 2006) was carried out at a sampling resolution of 1 or 2 cm from core GC01. For each sample, 1 cm^3 of sediment was soaked in distilled water overnight to disaggregate the sediment before washing through a 500 and 63 μm mesh (Scott et al., 2001). Specimens were identified and counted under suspension in distilled water using a Leica light microscope.

3.6. Radiocarbon dating

Twelve radiocarbon dates were determined from core GC01. The position of radiocarbon dates was chosen based on presence of calcareous foraminifera as well as targeting specific sections of the core showing clear changes in proxies measured. Depending on abundance of foraminifera, either benthic species (predominantly *Cassidulina neoteretis*) or planktonic species (*Neogloboquadrina pachyderma)* were used for dating. For one sample only (126–128 cm) that had low foraminiferal abundance, a date was obtained from a mix of benthic and planktonic species.

Accelerator mass spectroscopy (AMS) radiocarbon analysis on graphite (BETA Analytic) was undertaken where foraminifera were more abundant using between 4 and 10 mg of foraminifera, after pre-treatment with sonication in de-ionised water. Radiocarbon dating where foraminifera were less abundant was undertaken at the Laboratory for the Analysis of Radiocarbon (University of Bern) using between 0.4 and 1.5 mg of sample utilising the MIni CArbon DAting System (MICADAS) AMS. The latter allows analysis in gas form (CO_2), without the need for graphitisation, and hence allows for much smaller sample sizes whilst still being accurate and reproducible (Gottschalk et al., 2018; Missiaen et al., 2020; Szidat et al., 2014).

Direct radiocarbon age calibration was performed in Calib 8.2 software using the MARINE20 calibration curve (SM 2). It has been noted that there are issues regarding using the MARINE20 calibration in polar locations (Heaton et al., 2020; Reimer et al., 2013, 2020; Stuiver et al., 2020). In order to acknowledge this issue in the development of our age-depth model, we calibrate using both a Holocene reservoir correction (ΔR) consistent with previous studies (upper age boundary) and a glacial reservoir correction (ΔR_G) based on a model re-creating reservoir ages at higher lattitudes (lower age boundary) (Heaton et al., 2022, 2023).

To do this we create two separate age-depth models using the BACON age modelling package in R (SM 3) (Blaauw and Christen, 2011; Reimer et al., 2013; Stuiver et al., 2020). The first age-depth model was calibrated to MARINE20 using a ΔR of −10 ± 30 years. The choice to use a ΔR of −10 ± 30 years was made to be in keeping with previous regional studies using the MARINE13 calibration curve and a ΔR of 140 ± 30 years, which was done by subtracting 150 years to account for the mean offset between MARINE13 and MARINE20 (Heaton et al., 2023; Jackson et al., 2017; Jennings et al.,

2014, 2018). The second age-depth model was calibrated to MARINE20 and included all ages older than 11,500 cal years (i.e. all pre-Holocene ages) (Heaton et al., 2022) using a ΔR_G of 1240 ± 30 years. This is calculated by adding an additional 1250 to the original ΔR of −10 ± 30 years based on a latitude of ~70° N (Fig. 3 of Heaton et al., 2022). Using these upper and lower age boundaries a single age-depth model was developed by averaging the mean ages from both the Holocene and glacial reservoir corrected age-depth models (SM 2, 3).

In both scenarios the BACON models included boundaries placed at 22 cm and 122 cm to distinguish between estimated average sedimentation rates (480, 30, 350 yr per cm). Due to low foraminifera abundances, this study uses samples of both benthic and planktonic foraminifera, with some mixed samples, to achieve enough material for dating. In a previous study from Baffin Bay, this issue is investigated through varying reservoir ages whilst also looking at the difference between benthic and planktonic foraminifera ages (Jackson et al., 2017). The authors found that, while this led to changes in calibrated ages, they were still within the 95% confidence limits of the BACON-derived age model (Jackson et al., 2017). Therefore, we consider that the choice to use the same reservoir age correction for the benthic and planktonic foraminifera samples used in this study is justified, and in keeping with previous studies in the area (Jackson et al., 2017; Jennings et al., 2014, 2018). Although we attempt to address the calibration issues associated with high lattitudes, caution should still be used when comparing the age model here with other studies and proxies (Blaauw, 2012).

3.7. Lithogeochemistry

A Geoteck multi-core scanner (Dept. Geography, Durham) was used to obtain X-ray fluorescence (XRF) data on core GC01 at a resolution of ≤100 μm. The core surface XRF data was obtained by the bombardment of high energy x-rays (15 W/50 kV) generated in a rhodium x-ray tube, with x-ray detection using a Canberra Silicon Drift Detector. To improve the sensitivity of light element determinations (e.g., calcium, magnesium, aluminium, and silicon), the measurement cell was flushed with helium.

A representative suite of 1 cm stratigraphic intervals (N = 23) from GC01 were analysed for major, trace and rare earth elements (REEs) to aid in determining sediment provenance. These were analysed using a combination of fusion inductively coupled plasma mass spectrometry (ICP-MS) and total digestion (TD) ICP-MS by Activation Laboratories following standard analytical protocols (4Lithores − research). The same set of analysis was also undertaken for 10 Paleozoic carbonate rock samples (Fig. 1) to understand the chemical composition of the carbonate detritus. Detection limits for the 4Lithores research analysis are low ppm/ppb for most trace elements. Standards and duplicates analyses are within a few ppm for most of the elements.

qXRD analysis was performed using established protocols in order to reveal potential sediment sources (Andrews, 2019; Andrews et al., 2018; Andrews and Eberl, 2011; Eberl, 2003). In brief, qXRD was determined on the <2 mm sediment fraction of 25 samples over the length of GC01 with an interval spacing between 4 and 9 cm. The samples were measured on a Siemens D5000 XRD unit between 5 and 65 2-theta at a 0.02 2-theta step with a 2 s count, resulting in 3000 data points. The XRD data was imported into the Excel macro-program Rockjock v6 to quantify the wt. % of thirty-three nonclay and clay minerals including alkali-feldspars, plagioclase, dolomite and illite minerals, which were then normalised to sum to 100%. This method is ranked 3rd in the international Reynold Cup, whereby the results are tested against artificial known mineral mixtures (McCarty, 2002). The average bias on a mixture of 11 common minerals (bias = abs [Measured wt. % − Estimated qXRD wt. %]) was ±1 wt %.

3.8. Rhenium-osmium (Re−Os) isotope analysis

Rhenium-Os analysis was carried out from the cores of GC01 (N = 77), BC06 (N = 1) and 31 P (N = 21). The Re−Os analysis is based on established procedures (Selby and Creaser, 2003) and conducted in the Durham Geochemistry Centre (Dept. Earth Sciences) to obtain the hydrogenous (sequestered from water) Os isotopic composition ($^{187}Os/^{188}Os$) of the sediment sample, which records the $^{187}Os/^{188}Os$ of seawater at the time of deposition. In brief, ~1 g of dried, sieved and powdered sample (recording 1 cm of stratigraphy) is sealed into a Carius tube with 8 mL CrO_3 4 N H_2SO_4 and a known amount of tracer solution ($^{185}Re + {}^{190}Os$) and heated at 220 °C for 48 h. The Carius tubes are opened, and a solvent extraction using 9 mL chloroform ($CHCl_3$) separates the Os that is then back extracted into 3 mL HBr. The Os fraction is further purified by H_2SO_4−CrO_3−HBr microdistillation. The Re fraction is obtained from the Os extracted CrO_3−H_2SO_4 solution using a NaOH (5 N) -acetone extraction and is purified using HCl−HNO_3 anion bead chromatography.

Two samples from core GC01 that represent the peak in Ca and $^{187}Os/^{188}Os$ at 67.5 cm and 32.5 cm were also analysed following removal of the carbonate matrix. Two aliquots of each sample depth were analysed (2 × 67.5 cm and 2 × 32.5 cm). One aliquot from each depth was reacted with 1 N HCl and the other aliquot from each depth with 2 N HCl, 1 mL at a time, and shaken until the reaction ceased (5 mL total). The samples were centrifuged and the HCl was then removed, and the remaining sediment washed 3 times using 2 mL MQ. The remaining dried sediment then underwent Re−Os analysis as described above.

The Re and Os fractions were loaded onto Ni and Pt filaments, respectively and analysed using a ThermoScientific TRITON mass spectrometer using negative thermal ionisation mass spectrometry (NTIMS).

Seven of the Paleozoic carbonate rock samples (Fig. 1) and five larger clasts found within core GC01 (both carbonates and granites/gneisses), were also analysed to establish the whole rock Re−Os abundance and isotope composition. This followed the same method as described above using inverse aqua regia (3 mL 11 N HCl, 6 mL 15.5 N HNO_3) to permit whole rock digestion, with sample digestion at 220 °C for ~72 h to aid full digestion (Shirey and Walker, 1998).

Total analytical protocol blanks are similar throughout the study (Re = 15.97 ± 6.26 ppt, Os = 0.10 ± 0.07 ppt, with a $^{187}Os/^{188}Os$ of 0.23 ± 0.22; 1 S.D., N = 8), as are aqua regia blanks (Re = 4.48 ± 0.68 ppt, Os = 0.03 ± 0.02 ppt, with a $^{187}Os/^{188}Os$ of 0.14 ± 0.02; 1 S.D., N = 3). To monitor the long-term reproducibility of the Re−Os isotope composition determinations, Re and Os solution standards were routinely analysed. A 50 pg osmium standard solution (DROsS - Durham Romil Osmium Standard) gives $^{187}Os/^{188}Os$ values of 0.16074 ± 0.00026 (1 S.D., N = 26), which is in agreement with proposed values for the solution and the laboratory running average (0.16082 ± 0.00063 1 S.D; N = 816; (Luguet et al., 2008). The 125 pg rhenium standard solution (Restd) yields $^{185}Re/^{187}Re$ values of 0.59855 ± 0.00096 (1 S.D., N = 26), which agrees with the laboratory running average (0.59861 ± 0.0015 1 S.D; N = 720).

3.9. Mixing model

The discussion refers to a mixing model to help determine whether the radiogenic $^{187}Os/^{188}Os$ values recorded in core GC01 could be achieved with a sediment source from the Paleozoic carbonate rocks analysed in this study (Fig. 1). The two-component

mixing model uses seawater and carbonate rock as end members. The model requires input of both the $^{187}Os/^{188}Os$ value and Os concentration in each component. Using equations 2 to 11 listed on page 7 of van der Ploeg et al. (2018), the model calculates what percentage of osmium flux into Baffin Bay would be needed from a carbonate rock source to increase the seawater $^{187}Os/^{188}Os$ and total Os values to the highly radiogenic $^{187}Os/^{188}Os$ intervals recorded in the core sediments.

3.10. Carbonate correction

In this study, some of the major element, oxide and REE data is carbonate corrected over the detrital carbonate layers recorded in the Baffin Bay core (GC01). This was done to remove the effect of carbonate dilution on the datasets to see any trends in the data not caused by a large influx of carbonate material. To do this, the percentage carbonate of each peak and the background carbonate percent must be known, as well as the average element/oxide/REE concentration/% in the carbonate rocks and the core sediments. The effect of the carbonate dilution is then removed using the equation:

$$\left(\frac{(100-A)\times((B\times 100)-(C\times D))}{(100-C)+(A\times D)}\right)\div 100 = E$$

where: A = the background carbonate %; B = chosen element value (ppm/%) at a chosen core depth (to be corrected); C = % carbonate at chosen core depth; D = the average chosen element value (ppm/%) of the carbonate rock, E = carbonate corrected chosen element value (ppm/%).

4. Results

4.1. Core sedimentology and PSA

Between 168 and 120 cm GC01 consists of brown to dark brown massive sandy silt. Between these depths the grain size is the most variable, with sand content between 0.4 and 82%, silt content between 35 and 91%, and clay content between 3.5 and 18% (Fig. 2; S4). Moving up the core the sedimentology alters to light-brown massive clayey-silts (122–108 cm) followed by a sharp, curved contact to mid-to dark brown sandy silty sediments up to 86 cm. Between 86 and 76 cm light brown massive, clayey and silty sediments are found before a distinct change to light brown to cream coloured massive diamicton (76–59 cm). Between 59 and 42 cm the sediments consist of grey to mid-brown, lightly laminated sandy to clayey silts before a change back to light brown to cream coloured diamicton between 42 and 22 cm. From here to the core top the sediments are mid-brown, lightly laminated sandy silts moving to darker brown, lightly laminated more clay rich sediments. Between 120 cm and the core top, the sand contant varies between 10 and 38%, the silt content between 51 and 76% and the clay content between 9 and 33%.

4.2. X-ray and IRD

The X-ray images reveal density variations relating to the sedimentology as discussed above (Fig. 2). For example, a darker x-ray image is seen between 76 – 59 cm and 42–22 cm corresponding to the lighter coloured diamicton and the curved contact is clearly seen ~108 cm. Between 168 and 105 cm, no IRD is present except for small amounts between 130 and 120 cm. An increase in IRD, up to 6 clasts per 2 cm slice are found between 105 and 86 cm (Fig. 2). After a distinct absence (86–76 cm) IRD between 76 cm and the core top, with peaks between 76 and 59 cm and between 42 and 22 cm.

4.3. TOC

TOC values remain fairly constant through the core at ~0.1–0.6% with the exception of two peaks between 76 and 59 cm (2.8%) and between 42 and 22 cm (3.8%).

4.4. Foraminifera

The target foraminiferal count was 300 specimens per sample, however, for many samples this was not possible, with many samples having less than 100 specimens and some being barren. The benthic and planktic species diversity is very low. The benthic foraminiferal fauna is dominated by *Cassidulina neoteretis,* with *Trioculina* spp also common. Planktonic foraminifera are also common in some sections of the core dominated by *Neogloboquadrina pachyderma* (S5) (Codling, 2017). Foraminifera abundance is generally low between 168 and 120 cm and very low to zero from 25 to 0 cm (Fig. 2). Increased foraminifera abundance occurs between 120 and 95 cm (>2000 individuals per 4 mL; predominantly planktics), 75 and 55 cm (up to ~560 individuals per 4 mL; predominantly planktics), and between 45 and 25 cm (up to ~680 individuals per 4 mL; predominantly benthics).

4.5. Radiocarbon dates and age modelling

The age-depth model developed indicates GC01 records ~36 kyrs of sedimentation from the Late Quaternary through the Holocene to the present day (Fig. 3; S2, 3). The sedimentary record covers several significant events in the Baffin Bay region including the LGM, BBDC 4 to 0, the Bølling-Allerød, the Younger Dryas and the transition to the Holocene (Jackson et al., 2017; Rasmussen et al., 2006; Simon et al., 2014).

4.6. Lithogeochemistry

4.6.1. Core GC01

All data for XRF, XRD, REE and trace element analysis can be found in the supplementary materials (S6-12). From the full range of XRF data, here we present and discuss only the calcium (Ca) data as a direct proxy for carbonate content to identify the BBDC layers. The Ca counts per second (cps) vary between 1500 and 25,000 cps (Fig. 4). Between 164 and 80 cm Ca cps are relatively low and constant (approximately 5000 cps) with the exception of peaks between ~146 and 136 cm (13,000 cps), ~134 and 128 cm (10,000 cps), ~127 and 123 cm (9400 cps), ~111 and 101 cm (7700 cps), and 101 and 90 cm (7500 cps). At ~76 cm a peak to 15,400 cps leads to the highest peak in Ca (25,000 cps) between ~77 and 60 cm. The second largest peak in Ca (20,000 cps) occurs in between ~42 and 24 cm. From 22 cm to present day, Ca cps gradually decrease (7300–1900 cps). The two large Ca peaks at ~77–60 and ~42–24 cm are matched by peaks in CaO% of 15 and 17%, respectively (Fig. 4), and peaks in XRD calcite and dolomite % to 33.5 and 37.5%, respectively (Fig. 4).

The major-element oxide, trace element and REE data is carbonate corrected for the sediments taken from the Ca-rich depths (~77–60 cm and ~42–24 cm). The carbonate correction is based on the average elemental-oxide values and average REE values for the analysed Palaeozoic carbonate rocks (see methods) which are considered representative of the Paleozoic carbonates on the Canadian Islands and inter-island marine channel floors, represent the most likely origin of the detrital carbonate layers in Baffin Bay (Fig. 1) (Andrews, 1987; Andrews et al., 1998; Andrews and Eberl, 2011; Simon et al., 2014).

The La/Sc ratio mirrors Ca concentration, being relatively constant (3.5–2.5) with the exception of two peaks to 5.6 (77–60 cm)

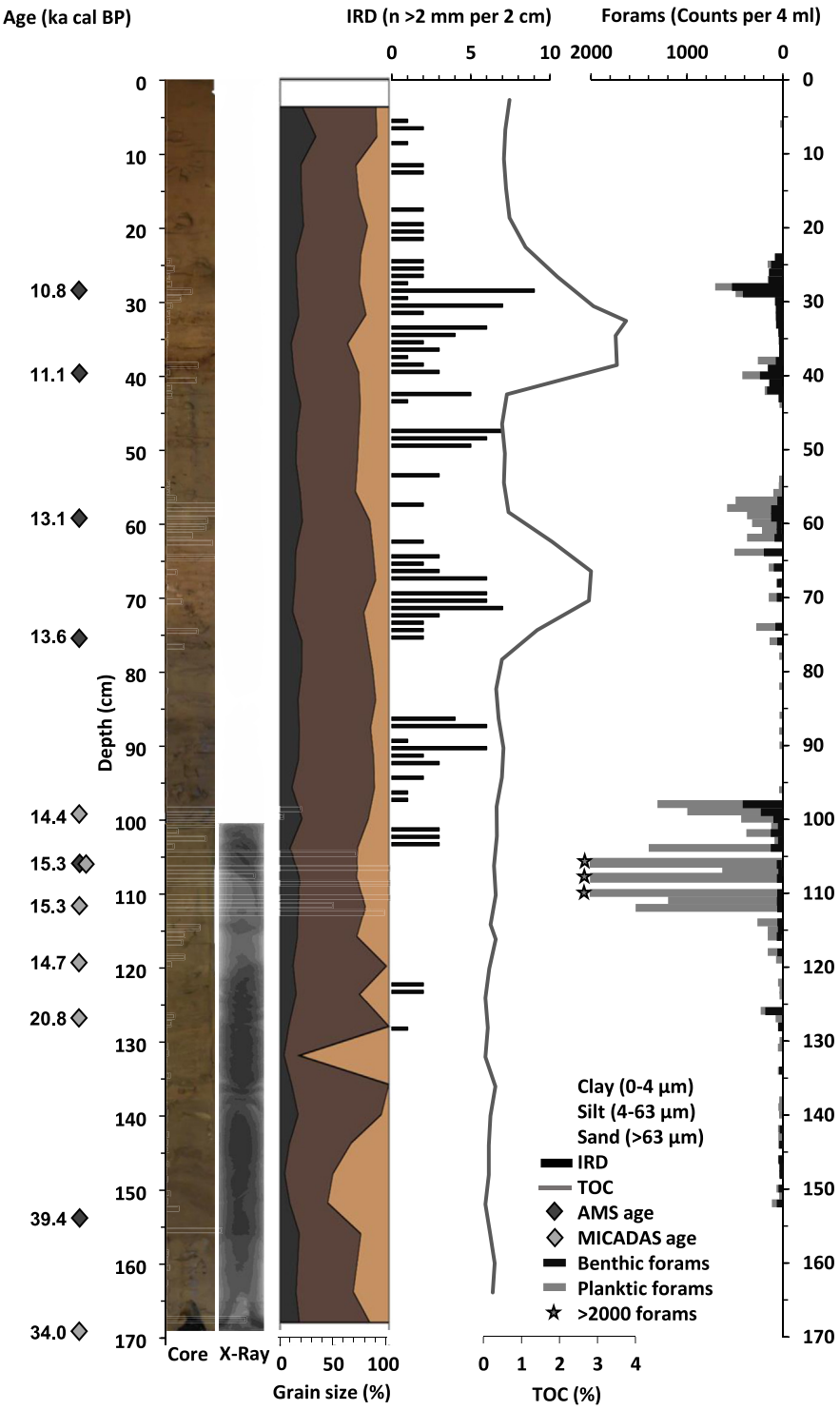

Fig. 2. Physical properties of core GC01. Properties include core and X-ray photos, grain size (%), IRD (n > 2 mm per 2 cm core slice), foraminifera (counts per 4 mL) and TOC (%) against depth (cm) for GC01. Position of radiocarbon dates also indicated (cal ka BP). Dark coloured diamonds next to the radiocarbon age indicate calibrated ^{14}C AMS ages and light-coloured diamonds indicates calibrated ^{14}C MICADAS AMS ages. The ages are an average of the Holocene ($\Delta R = -10 \pm 30$) and glacial ($\Delta R_G = 1240 \pm 30$) calibrated ages for each depth (S2).

and 5.0 (45–21 cm) (Fig. 4), indicative of a predominantly felsic detrital provenance (Bhatia and Crook, 1986; Selby et al., 1999; Taylor and McLennan, 1985). Similarly, both SiO_2/Al_2O_3 and K_2O/Na_2O are relatively stable across GC01 (~4.4–3.6 and 0.7 to 1.4, respectively) except for peaks between 76 and 58 cm (5.8 and 1.4, respectively) and 44 and 20 cm (5.7 and 1.3, respectively; S13). The SiO_2/Al_2O_3 and K_2O/Na_2O data predominantly indicate a greywacke composition, with a few depth intervals bearing a more litharenite

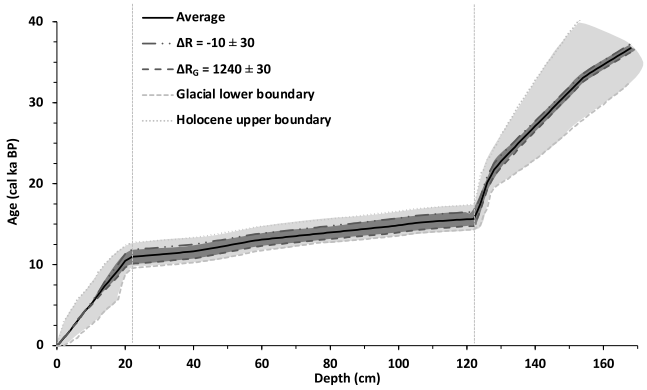

Fig. 3. Age model developed for core GC01. Calibrated using the MARINE20 curve and the Bayesian modelling of radiocarbon dates using the BACON software (see methods). The dark grey dashed lines labelled $\Delta R = -10 \pm 30$ and $\Delta R_G = 1240 \pm 30$ represent the age-depth models developed individualy by BACON using the two different reservoir corrections, the Holocene and glacial corrections, respectively. The solid black line, labelled average, is the average of these two age models, and therefore the age-depth model used in discussion in this study. The outer lighter grey dashed lines represent the upper age boundary of the Holocene reservoir correction, and the lower age boundary of the glacial reservoir correction, in order to show a greater range of ages. Dashed vertical grey lines indicate boundaries placed at 22 cm and 122 cm in the BACON model to distinguish between averaged sedimentation rates and a potential hiatus at ~122 cm. Between 0 and 22 cm the average sedimentation rate is 2.6 cm/kyr, between 22 and 122 cm this increases to 23.5 cm/kyr, and between 122 cm to the core bottom this decreases back to 2.0 cm/kyr.

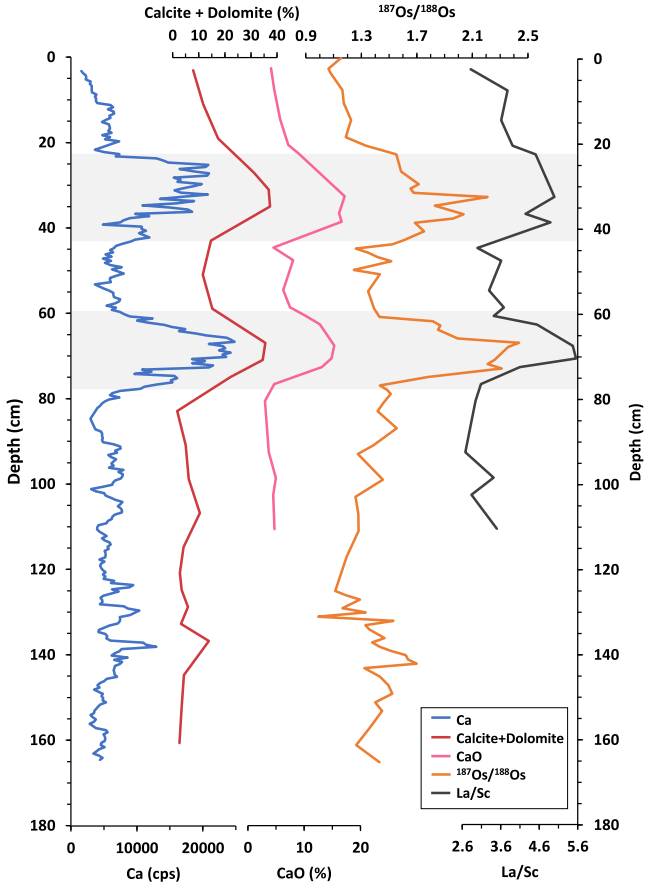

Fig. 4. Multiproxy datasets for GC01 presented against depth. Ca (cps), Calcite + dolomite (%), CaO (%), ^{187}Os/^{188}Os, and La/Sc for GC01 plotted against depth. Shaded areas represent areas of significant peaks. See text for discussion.

composition (e.g., 98.5, 72.5, 70.5 and 67.5 cm) (Pettijohn et al., 1987).

Carbonate corrected REE values for GC01 samples are normalised to upper continental crust and chondrite values (McLennan, 2001). All sediments analysed illustrate light REEs (LREEs) enrichment relative to upper crust and chondrite values, with Eu anomalies (Fig. 5). Overall, the REE and trace element (e.g., La/Sc) data support a felsic, continental crust provenance. The slight variations relative to average upper continental crust may imply slight differences in the felsic detrital provenance.

4.6.2. *Paleozoic carbonate rocks*

The carbonate rocks from Somerset and Devon Islands contain on average high CaO (31.7%), MgO (16.8%), with low SiO_2 (4.92%), and <1% of TiO_2, Fe_2O_3, Al_2O_3, P_2O_5, Na_2O, K_2O, and MnO. The La/Sc ratio average is 3.8 (range 2.6–4.8) based on the three samples where Sc was above detection (1 ppm). Except for four samples, the REE data exhibit flat profiles relative to chondrite and upper continental crust, with the remaining four samples displaying moderate enrichment in LREE relative to HREE.

4.7. *Re and Os abundance and Os-isotope composition*

For GC01, the Re abundance ranges between ~0.2 and 0.4 ppb, with the exception for two peaks of 4–5 ppb between ~98 and 71 cm and ~62 to 39 cm. The total Os abundance ranges between 8.9 and 111 ppt, with abundances commonly between ~20 and 50 ppt, except for intervals between 164 and 157 cm, at 117 cm, between 92 and 77 cm, ~44 cm and 14 to 0 cm where values are between 75 and 111 ppt (S13; S14A).

Given the relatively young age and low rhenium abundance of the sediments of all core samples, the correction for any ingrowth of radiogenic ^{187}Os to the measured present-day ^{187}Os/^{188}Os composition is less than that of the minimum ^{187}Os/^{188}Os uncertainty (~0.01). Therefore, the uncorrected, measured present-day ^{187}Os/^{188}Os compositions are discussed. The ^{187}Os/^{188}Os compositions range between 0.99 and 2.44 (Figs. 4 and 6).

For GC01, the ^{187}Os/^{188}Os values from the bottom of the core to ~125 cm gradually decrease except for an abrupt increase to 1.7 at 142 cm and decrease to a more unradiogenic value of 0.99 at ~131 cm. Between 125 and 78 cm, ^{187}Os/^{188}Os values gradually increase (1.2–1.5). Between ~78 and 60 cm, the ^{187}Os/^{188}Os rapidly peak to highly radiogenic values of 2.44 before abruptly returning to 1.43 (Figs. 4 and 6). Values remain relatively stable at approximately 1.3–1.4 from 60 to 50 cm. Between ~50 and 19 cm ^{187}Os/^{188}Os show a rapid increase to 2.21, followed by an abrupt decrease to 1.65 (~32 cm), before a steady decrease to 1.33. Between 19 cm and the core top, ^{187}Os/^{188}Os values gradually decrease from 1.33 to 1.15.

To ascertain if the carbonate matrix of the high Ca intervals is the cause of the highly radiogenic compositions of the GC01 sediments (above), a leach experiment was undertaken. For the sample at 67.5 cm, the 1 N and 2 N HCl leach removed 26 and 42% of the carbonate mass, which is similar to the determined carbonate value of the interval (Fig. 4; S14C). The 1 and 2 N HCl leached sediment is more enriched in Os (29.0 and 24.6 ppt total Os; 9.1 and 7.6 ppt ^{192}Os), and slightly more radiogenic (^{187}Os/^{188}Os = 2.60 and 2.67), in comparison to the non-leached sediment analysis (Total Os = 20.1 ppt, ^{192}Os = 6.4, ^{187}Os/^{188}Os = 2.40; S14A, C). For the sample at 32.5 cm, the 1 N and 2 N HCl removed 27 and 46% of the carbonate mass, which is similar to the determined carbonate value of the interval (Fig. 4; S14C). The 1 N HCl leached sediment is more enriched in Os (34.3 ppt total Os; 11.4 ppt ^{192}Os/the 2 N sample was lost during processing), and slightly less radiogenic (^{187}Os/^{188}Os = 1.99) in comparison to the non-leached sediment

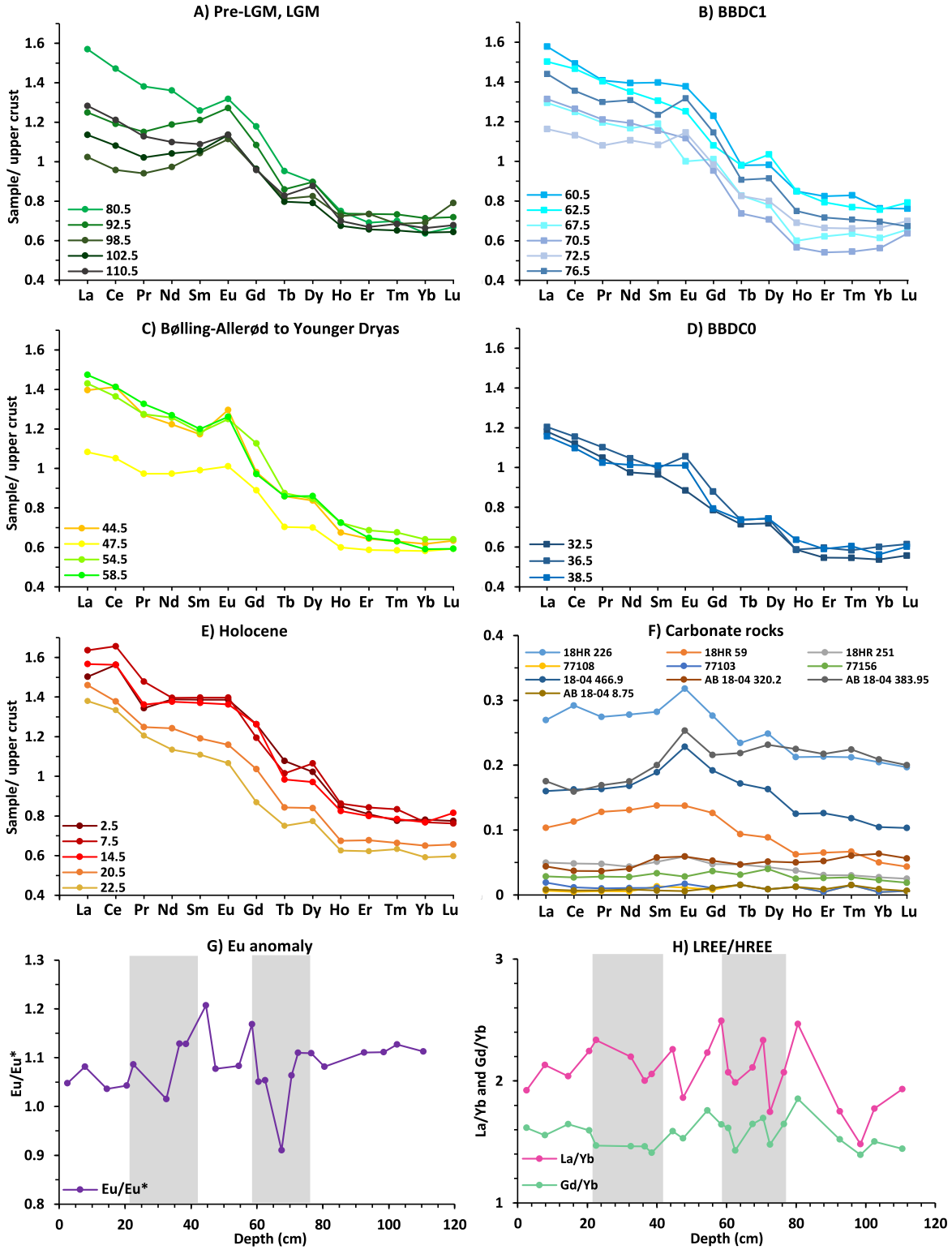

Fig. 5. Normalised REE data for GC01 and carbonate rocks. REE data normalised to upper crust plotted for the depths corresponding to (A) Pre-LGM and LGM (linked together as other data sets such as Ca and $^{187}Os/^{188}Os$ are relatively similar in comparison to other intervals), (B) BBDC1, (C) the transition from the end of the Bølling-Allerød into the Younger Dryas, inbetween BBDC layers, (D) BBDC0, (E) the Holocene, (F) REE data for each carbonate sample analysed from Somerset and Devon Islands. (G) the europium anomaly values (Eu/Eu*) in GC01, and (H) the light rare earth element/heavy rare earth element (LREE/HREE) ratio in the form of La/Yb_N and Gd/Yb_N for GC01. The grey shaded region denotes BBDC1 (76–59 cm) and BBDC0 (42–22 cm).

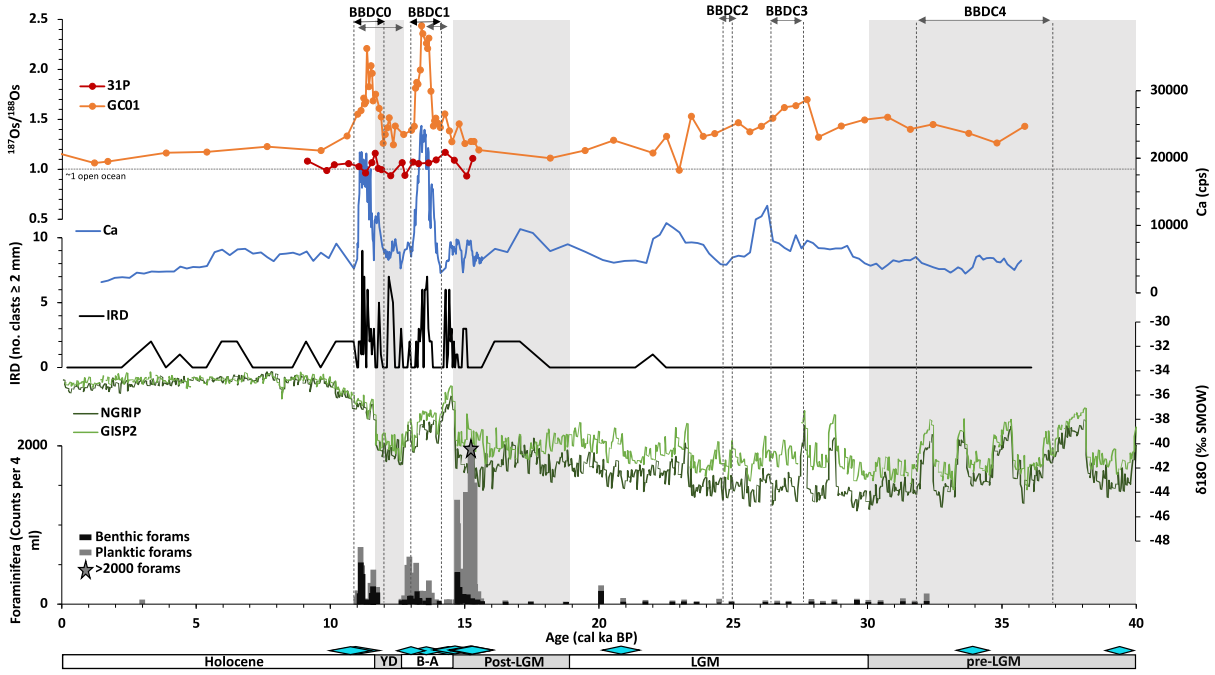

Fig. 6. Osmium isotope data, carbonate proxy data, and ice core oxygen isotope data presented against age. $^{187}Os/^{188}Os$, Ca (cps), IRD (no. clasts ≥2 mm per 2 cm core slice) and foram (counts per 4 mL) data from core GC01, $^{187}Os/^{188}Os$ for core 31 P, and ice core $\delta^{18}O$ values from NGRIP and GISP2 plotted against the age model determined in Fig. 3. NGRIP and GISP2 ages were corrected from years B2k to years BP to fit with the age model (Rasmussen et al., 2014; Seierstad et al., 2014; Stuiver and Grootes, 2000). The width of the blue diamonds show the age range between the median probabilities of the Holocene reservoir correction and the glacial reservoir correction (S2). Dashed lines are previous approximate ages of the Baffin Bay detrital carbonate layers BBDC4, BBDC3 and BBDC2 (Andrews et al., 1998; Jackson et al., 2017; Simon et al., 2014). The dashed lines and black arrows of BBDC0 and BBDC1 respresent our new proposed timings for these layers, lighter grey arrows underneath show their approximate ages based on previous literature as a comparison. Horizontal dashed line shows the open ocean average value for $^{187}Os/^{188}Os$ of 1. The grey and white bar and shading shows the approximate timings of the pre-Last Glacial Maximum (LGM), LGM, post LGM, the Bølling-Allerød, Younger Dryas and the Holocene (Clark et al., 2009; Jennings et al., 2017; Ó Cofaigh et al., 2019, 2013b). See text for discussion.

analysis (Total Os = 20.1 ppt, ^{192}Os = 6.5, $^{187}Os/^{188}Os$ = 2.20; S14A, C).

The carbonate clasts recovered from GC01 at depths of 70, 38, 29.5 and 8.5 cm range in Re and Os abundance between 0.04 and 0.18 ppb, and 5.3–48.8 ppt, respectively, with $^{187}Os/^{188}Os$ between 0.40 and 3.34 (Table 1). A single granitic clast (comprising feldspar and quartz) from 71 cm possesses a Re abundance of 0.09 ppb and Os of 16.5 ppt, with a $^{187}Os/^{188}Os$ of 1.29.

The Paleozoic carbonate rock samples possess Re and total Os abundances between 0.03 and 0.36 ppb, and 1.21 and 16.48 ppt, respectively, with $^{187}Os/^{188}Os$ between 1.03 and 9.51 (Table 1). The average $^{187}Os/^{188}Os$ of these samples is 2.85 ± 2.49, although this reduces to 2.19 ± 1.21 if the single most radiogenic sample of 9.51 is removed.

Table 1
Re–Os data of rocks and clasts around Baffin Bay. $^{187}Os/^{188}Os$ data from Paleozoic carbonate rock samples from Somerset and Devon Islands (Fig. 1) analysed in this study, and from clast samples found within core GC01 analysed in this study. Also shown is a metagreywake, basalt (average of two repeats) and gneiss from areas surrounding Uummannaq Fjord, west Greenland (Rooney et al., 2016). Uncertainty is ±2 SE. See S14B for complete data synopsis and S1 for location information.

Type	Sample	Depth (cm)	Re (ppb)	±	Os (ppt)	±	$^{187}Os/^{188}Os$	±
Carbonate rock	**AB18–01 466.9**	–	0.36	0.00	11.43	0.27	2.40	0.14
	AB18–01 320.2	–	0.03	0.00	5.52	0.15	3.64	0.23
	AB18–01 383.95	–	0.05	0.00	16.48	0.40	2.91	0.17
	18HR251	–	0.08	0.00	7.49	0.16	1.03	0.06
	18HR226	–	0.27	0.00	7.99	0.19	2.26	0.14
	77108	–	0.04	0.00	1.21	0.06	3.60	0.48
	77156	–	0.23	0.00	4.54	0.17	9.51	0.72
Carbonate clast	**8-9 cm W Carb**	8.5	0.04	0.00	12.81	0.26	0.73	0.04
Carbonate clast	**29–30 cm A Carb**	29.5	0.06	0.00	48.82	0.91	0.40	0.02
Carbonate clast	**38 cm W Carb**	38	0.14	0.00	5.28	0.16	3.34	0.25
Carbonate clast	**70 cm W Carb**	70	0.18	0.00	14.63	0.32	1.55	0.09
Granite clast	**71 cm A Granite**	71	0.09	0.00	16.53	0.35	1.29	0.07
Uummannaq Fjord samples	**Metagreywacke**	–	0.04	0.00	85.80	1.60	0.44	0.03
	Gneiss	–	0.00	0.00	1.60	0.00	2.82	0.16
	Basalt	–	0.20	0.00	19.00	0.30	1.34	0.05

Samples between 40 and 160 cm (15.3–9.1 cal ka BP) from core 31 P possess Re and total Os abundances between 0.45 and 11.4 ppb, and 30.2 and 74.5 ppt, respectively (S14A), with $^{187}Os/^{188}Os$ between 0.93 and 1.17 (Fig. 6).

5. Discussion

5.1. Pre-Last Glacial Maximum (LGM; 36–30 cal ka BP)

Between ~36 and 30 cal ka BP the $^{187}Os/^{188}Os$ values (1.3–1.5) are more radiogenic than the open ocean at the time (~1; Fig. 6) (Paquay and Ravizza, 2012; Peucker-Ehrenbrink and Ravizza, 2000) suggesting some limited flux of radiogenic materials from the surrounding old, continental geologies (Fig. 1) (Rooney et al., 2016). At this time ice sheets surrounding Baffin Bay were yet to reach their most extensive position at the continental shelf edges (Andrews et al., 2015; Briner et al., 2003; Dalton et al., 2020; Knutz et al., 2019; Ó Cofaigh et al., 2013b). During this time $^{187}Os/^{188}Os$ values and Ca counts are relatively stable, no IRD is present and foraminiferal abundances are generally low (Fig. 6). These factors suggest a steady outwash of material into Baffin Bay through meltwater and glacio-fluvial sediment delivery, with no evidence of significant 'events' such as major iceberg rafting associated with ice sheet dynamics. This time period also covers the proposed timing of BBDC4 (~37–31.9 cal ka BP) (Jackson et al., 2017; Simon et al., 2014), as well as a number of fluctuations in $\delta^{18}O$ seen in the ice core records (Fig. 6) (Rasmussen et al., 2014; Seierstad et al., 2014; Stuiver and Grootes, 2000). Based on the wide range of proxies presented here (and taking into account age differences due to different radiocarbon calibration methods), there is no evidence of BBDC4 in the sedimentary sequence of GC01. However, it is possible that this may be due to relatively low sampling resolution with a less well constrained age model in this section of the core.

5.2. LGM (~30–19 cal ka BP)

At ~28 cal ka BP there is an abrupt increase and then more gradual decrease in $^{187}Os/^{188}Os$ values to the end of the LGM (~19 cal ka BP; Fig. 6). This abrupt change indicates an influx of more radiogenic Os, most likely from the Archean and Proterozoic aged gneisses and granites of west Greenland and Baffin Island, covered by the Greenland and Laurentide ice sheets, respectively (Fig. 1). This $^{187}Os/^{188}Os$ peak coincides roughly with the timing of maximum ice sheet advance onto the continental shelves of Baffin Bay (Batchelor et al., 2019; Briner et al., 2003; Clark et al., 2009; Dalton et al., 2022). At this time the core site would have been more proximal to the ice margins and affected by ice stream discharge into central Baffin Bay. A similar rise in $^{187}Os/^{188}Os$ composition in response to advance of a GIS ice stream (Jakobshavns Isbrae) has been reported during the Holocene in Disko Bugt (Rooney et al., 2016). Therefore, advance of the GIS/LIS ice margins to their LGM positions is the likely cause of the rise in $^{187}Os/^{188}Os$ composition (Fig. 6). The trend to less radiogenic $^{187}Os/^{188}Os$ from ~27 to 19 cal ka BP (Fig. 6) implies the gradual reduction in the flux of glacially eroded radiogenic $^{187}Os/^{188}Os$ material into the water column.

Minor increases in calcium occur during the LGM between 26.5 and 25.6 cal ka BP and 24.5 and 21.8 cal ka BP (Fig. 6). Previously dated timings of BBDC3 (~27.7–26.4 cal ka BP) and BBDC2 (~25–24.7 cal ka BP) are close to this range (Jackson et al., 2017; Simon et al., 2014). Taking into account the differences between age calibration in this study and the previous BBDC dates, the two Ca peaks identified may relate to these BBDC layers. However the age-model in this section is less well constrained due to low foraminiferal abundance. Low foraminiferal abundance suggests relatively low productivity during the LGM due to strong/stable, year-round sea ice cover and, hence, harsh sea surface conditions would be expected (Jennings et al., 2018). This also might explain the lack of IRD seen through this period (Figs. 4 and 6).

5.3. Post-LGM, Pre Bølling-Allerød (~19–14.7 cal ka BP)

The timing of the retreat of the GIS from the LGM maximum position is gradual and is considered diachronous across different outlets (Jennings et al., 2017; Sheldon et al., 2016; Simon et al., 2014). Retreat in the Uummannaq Trough is proposed to have been underway by 17.1 cal ka BP, whereas retreat in the Disko Trough (approx. 200 km south; Fig. 1) did not begin until 16.2 cal ka BP (Jennings et al., 2017). In the GC01 core, there is an abrupt increase in foraminiferal abundance, particularly planktic foraminifera, at ~15.7 cal ka BP (Fig. 6), indicating increased surface productivity potentially due to a reduction in sea ice concentration and also increased nutrient flux from melting/retreating ice sheets (Jennings et al., 2018). A similar large peak in both benthic and planktic foraminifera abundance preceding the Bølling-Allerød (~18 cal ka BP) has also been noted in a core from northern Disko trough mouth fan (core HU2008029–12 PC; Fig. 1) (Jennings et al., 2018). The difference in timing of the foraminifera peak from core GC01 is, in part, due to the altered radiocarbon calibration, but could also reflect the diachronous retreat of the sea ice margin/ice sheet(s) between Disko Bay (~18–17.5 cal ka BP) (Jennings et al., 2018) and the location of GC01 in central Baffin Bay (~15.7 cal ka BP) (Fig. 1).

IRD also increases at this time (~15.2 cal ka BP; Fig. 6) suggesting increased iceberg flux and melting to central Baffin Bay. This is further supported by $^{187}Os/^{188}Os$ compositions which begin to steadily increase from ~15.5 cal ka BP, implying an enhanced release of radiogenic Os from nearby Greenland sources (e.g., Uummannaq Fjord gneiss, $^{187}Os/^{188}Os = 2.82$; Table 1; Rooney et al., 2016).

Post-LGM Ca values do not correlate with variations in $^{187}Os/^{188}Os$ (Figs. 4 and 6). Assuming Ca can be used as a proxy for Paleozoic carbonate flux, the lack of significant variation in Ca counts supports relative stability along ice streams covering a predominantly carbonate geology in comparison to the GIS at this time (Jackson et al., 2017; Simon et al., 2014). This suggests different temporal ice sheet dynamics between ice streams from the IIS, LIS and the GIS. At this time it appears the northern LIS and southern IIS did not begin to deliver large quantities of icebergs carrying carbonate material to south Baffin Bay until after the initial GIS retreat at *c.* 17.1 cal ka BP. Perhaps remaining relatively stable for longer, or sea-ice in northern Baffin Bay could have prevented delivery of icebergs further south.

5.4. Bølling-Allerød (~14.7–12.9 cal ka BP), Younger Dryas (~12.9–11.7 cal ka BP) and early holocene (~11.7–10 cal ka BP)

A large peak in Ca occurs in GC01 during the Bølling-Allerød centred at ~13.5 cal ka BP (Fig. 6). This coincides with the previously dated timings of BBDC1 (14.2–13.7 cal ka BP) (Andrews, 1987; Andrews et al., 1998; Jackson et al., 2017; Simon et al., 2014). The Ca peak in GC01 coincides more tightly to the BBDC1 timings when calibrated to the MARINE13 curve (See S16 for comparison between MARINE13 and 20 age models) and hence this Ca peak is definitively identified as BBDC1. Using our updated age-depth model that takes into account the issues of polar calibrations (Heaton et al., 2022), we can now provide a new and improved age range for BBDC1 of 14.1–13.0 cal ka BP (Fig. 6). A second large Ca peak occurs just after the Younger Dryas, centred at ~11.2 cal ka BP (Fig. 6). This is coincident in timing with the latter part of the age range for BBDC0 of between ~12.7 and 12.4 cal ka BP lasting until ~11 cal ka BP (Andrews et al., 1998; Jackson et al., 2017). As with BBDC1, using our new age-depth model (Heaton et al., 2022) we can define a new age range for BBDC0 of ~12.0–10.9 cal ka BP. This new age range now defines BBDC0 as occurring synchronous with the end of the

Younger Dryas, rather than with the onset of the Younger Dryas as previously thought (Andrews et al., 1998; Jackson et al., 2017; Jennings et al., 2017; Rasmussen et al., 2006).

Coincident with both the Ca peaks over BBDC1 and BBDC0, there are also peaks in IRD, TOC, La/Sc, foraminifera and radiogenic $^{187}Os/^{188}Os$ (Figs. 4 and 6). Foraminifera abundance peaks at 13.0 cal ka BP after the initial decline in Ca and $^{187}Os/^{188}Os$ over BBDC1, and at ~11.2 cal ka BP coincident with BBDC0 (Fig. 6). The predominantly planktic BBDC1 peak could represent an increase in productivity in the surface waters due to the increased sediment and nutrient flux into Baffin Bay that occurred during BBDC1 and correlates to a similar peak in abundance in core HU2008029–12 PC at ~14 cal ka BP (Fig. 1) (Jennings et al., 2018). The predominantly benthic peak during BBDC0 indicates increased productivity most likely driven by increased nutrient delivery from glacial meltwaters. The increase in benthic productivity is most likely associated with an increased flux of food supply from surface productivity.

Pre ~15 cal ka BP, trends in $^{187}Os/^{188}Os$ and Ca are not synchronous, but for BBDC1 and BBDC0 there is a good correlation between the peaks in Ca and $^{187}Os/^{188}Os$. This could indicate the radiogenic $^{187}Os/^{188}Os$ signal is derived from the carbonate (carbonate mineralogy in core sediment is digested by Re–Os analytical protocol). Indeed, Re–Os analysis on carbonate rocks (Somerset and Devon Islands) yielded an average $^{187}Os/^{188}Os$ of 3.6 (range ~1.0–9.5; Table 1), which is more radiogenic than the highest $^{187}Os/^{188}Os$ value (2.44) recorded in the BBDC1 section of GC01 (Fig. 6). In the BBDC intervals, carbonate accounts for ~30–40% of the mineralogy (calcite + dolomite %; Fig. 4). Mass balance calculations using a two component mixing model (van der Ploeg et al., 2018) consider a carbonate sample with the most radiogenic $^{187}Os/^{188}Os$ composition (~9.5) and highest recorded Os abundance (16.5 ppt; Table 1), together with a seawater $^{187}Os/^{188}Os$ of ~1.3 (recorded prior to BBDC1 onset; Fig. 6). The results of this show that the carbonate content of the sediments over the BBDC intervals would have to exceed 71% to reach the most radiogenic values recorded in GC01 (2.44), significantly higher then the 30–40% shown by XRD. Thus, given the predominantly less radiogenic $^{187}Os/^{188}Os$ compositions, coupled with a lower Os abundance, of the carbonate lithologies from Somerset Island and IRD clasts in the core, an alternate source of more radiogenic osmium is required to account for the peak seen within the BBDC sediment layers in the core. Evidence of differing sources can also be inferred from the $^{187}Os/^{188}Os$ and Ca peaks themselves. Whilst for BBDC1 the $^{187}Os/^{188}Os$ and Ca peaks are broadly synchronous, during BBDC0 the $^{187}Os/^{188}Os$ decreases midway through the peak in Ca (Fig. 6). The initial rise in Ca is coupled with the $^{187}Os/^{188}Os$ rise suggesting a significant flux of material from the Paleozoic carbonates as well as ice streams from central-west GIS (and/or Baffin Island). However, at ~11.3 cal ka BP there is an abrupt decrease in $^{187}Os/^{188}Os$ followed by a more gradual decrease through to the early Holocene. In contrast, Ca levels remain high until ~11.0 cal ka BP, abruptly decreasing to their lowest values by 10.8 cal ka BP. The diverging trends between Ca and $^{187}Os/^{188}Os$ suggests a reduction in flux of material from radiogenic terranes (potentially from the GIS and/or Baffin Island LIS) and as sustained flux of detrital carbonate (NE LIS and S IIS). In addition to the mass balance modelling and a-synchronicity, REE data supports an additional source for the hydrogenous osmium signature, given that all REE abundances are significantly lower (most cases ~90% lower) in the carbonate rocks than they are across the whole core and the two BBDC layers (Fig. 5). The carbonate rocks also display no, or very little LREE enrichment, whereas the REE profiles during BBDC1 and BBDC0 in GC01 show high LREE enrichment (Fig. 5). Additional analysis of sediment leached of carbonate show that even after carbonate removal, samples GC01 67.5 cm and 32.5 cm retain radiogenic $^{187}Os/^{188}Os$ values of 2.60–2.67 and 1.99, respectively (S14C). Thus, the radiogenic $^{187}Os/^{188}Os$ values recorded during BBDC1 and BBDC0 cannot be as a result, at least wholly, of the carbonate matrix in sediment core sourced from Paleozoic carbonate rocks in the north and north-east of Baffin Bay (Fig. 1). Together, these differences between the analysed sediments and carbonate rocks suggest a significant additional provenance during this period, other than the dominant Paleozoic carbonate source. This provenance must therefore be from ice streams either of western Greenland (GIS) or Baffin Island (LIS). The geology of these areas, however, is very similar and, therefore, it is difficult to differentiate between sources (Aksu and Piper, 1979; Andrews et al., 2014; Harrison et al., 2011; Henriksen and Higgins, 2009; Jennings et al., 2018; Simon et al., 2014).

The $^{187}Os/^{188}Os$ record from core 31 P, further south in Davis Strait, records markedly less radiogenic values (0.9–1.2) compared to GC01 (1.4–2.4) over the same period covering BBDC1 and BBDC0 (Fig. 6). The lower $^{187}Os/^{188}Os$ values recorded in 31 P suggests a greater open ocean influence with less continental derived osmium input through the influence of advancing and retreating ice sheets, as noted at the same core site during the Holocene (Rooney et al., 2016).

5.5. Holocene (from ~11.0 cal ka BP – present)

After BBDC0, the Ca content in GC01 decreases abruptly, and then more gradually to the present day (Fig. 6). The $^{187}Os/^{188}Os$ values decrease more gradually but reach relatively unradiogenic and stable values by the early Holocene, with a gradual decrease to the present day, moving closer to open ocean values of ~1.0. This likely reflects a combination of an increased influence of open ocean waters through Davis Strait from the Atlantic via the West Greenland Current (similar $^{187}Os/^{188}Os$ values to those measured from 31 P at the onset of the Holocene) and a reduction in more radiogenic glacially eroded material as the ice sheets retreated back across the continental shelves around Baffin Bay (Hogan et al., 2016; Jennings et al., 2014; Ó Cofaigh et al., 2013b; Rooney et al., 2016). Further, the REE pattern during the Holocene does not record a positive Eu anomaly (relative to upper continental crust; Fig. 5) as seen in pre-Holocene lithofacies, suggesting reduced plagioclase and alkali feldspar input, and reduced glacial flux as the GIS and LIS retreat to, or inside of their current positions.

6. Provenance and significance of sediments during BBDC layers

It has previously been shown that the detrital carbonate in BBDC layers is sourced from the Paleozoic carbonate successsions located in the north of the bay, previously overlain by the NE LIS and southern IIS (Andrews, 1987; Andrews et al., 1998; Andrews and Eberl, 2011; Simon et al., 2014). Due to the size of the Lancaster Sound ice stream, it is thought that most of the carbonate material entered Baffin Bay via this ice stream (and other smaller ones in the north) with retreat into Lancaster Sound occurring by ~15.3 cal ka BP, preceding both BBDC1 and BBDC0 (Dalton et al., 2020, 2022; Furze et al., 2018; Kelleher et al., 2022).

However, based on the mixing model results discussed above, the source of radiogenic $^{187}Os/^{188}Os$ values during BBDC1 and BBDC0 cannot be wholly sourced from the Paleozic deposits supplying the carbonate material via e.g., the Lancaster Sound ice stream. Hence, there must be an additional source of radiogenic material most likely originating from the radiogenic terranes of west Greenland and/or Baffin Island, which again are difficult to differentiate due to similar geologies (Andrews et al., 2018;

Harrison et al., 2011; Henriksen and Higgins, 2009; Knutz et al., 2022; St-Onge et al., 2009).

Larger IRD clasts found in GC01 over BBDC1 and BBDC0 include both carbonate and granite/gneiss lithologies (Table 1). The granite/gneiss clast is less radiogenic ($^{187}Os/^{188}Os = 1.3$) than the host sediment ($^{187}Os/^{188}Os = 2.2$), which is also less radiogenic than the Archean orthogneiss from Salliaruseq Storøen Island ($^{187}Os/^{188}Os = 2.8$) (Rooney et al., 2016). However, the clast comprises only quartz and feldspar, and it is the preferential weathering of minerals such as biotite in crustal units that can ultimately lead to a water column possessing a radiogenic Os composition (Peucker-Ehrenbrink and Blum, 1998). The average $^{187}Os/^{188}Os$ of the carbonate clasts over these intervals is 1.76, lower than that in GC01 sediments and the clasts also contain lower abundances of Re and Os than the surrounding sediment (S13B).

The GC01 sediments over the BBDC layers also display LREE enrichment, positive Eu anomalies (relative to upper continental crust), and high La/Sc, SiO_2/Al_2O_3 and K_2O/Na_2O ratios compared to the carbonate rocks from Somerset and Devon Islands (Figs. 4 and 5; S13). This indicates a predominantly felsic provenance dominated by plagioclase and alkali feldspar (Bhatia and Crook, 1986; Taylor and McLennan, 1985) similar to the Precambrian crystalline rocks along the west coast of Greenland (Fig. 1). Sediment (with minimal carbonate) deposited proximal to the Jakobshavn Isbrae ice margin in Disko Bugt possesses a hydrogenous $^{187}Os/^{188}Os$ composition of ~2.0–2.4 during ice proximal conditions in comparison to ~1.3 to 1.8 during times when the ice margin was more distal (Rooney et al., 2016). This supports an interpretation that the radiogenic $^{187}Os/^{188}Os$ values of ~2.0–2.5 recorded during BBDC1 and BBDC0 in GC01 could be achieved solely by a western Greenland source. Further supporting this interpretation, a previous study using XRD and SedUnMix has linked the mineralogy of finer-grained glaciomarine sediments found within coarser BBDC layers to a west Greenland source, potentially linked to the Uummannaq trough ice stream (Simon et al., 2014). A study investigating the provenance of central Baffin Bay sediments based on lead, neodymium and strontium radiogenic isotopes determined that the isotope values during the last deglaciation (since the LGM) indicate source areas of central-west and south-west Greenland, mainly from the Nagssugtoqidian Mobile Belt and the Archean Block (Kirillova, 2017), again indicating the potential of a west Greenland source.

The physiography of Baffin Bay also indicates that ice streams from west Greenland are the most likely source of radiogenic sediment delivery to the core site. The continental shelf of west Greenland is wide (135–200 km), with a number of troughs leading to large trough mouth fans, compared to the narrower Baffin Island Shelf (25–50 km) with comparatively fewer and smaller troughs and trough mouth fans (Andrews et al., 2014; Harrison et al., 2011; Henriksen and Higgins, 2009; Knutz et al., 2019; Li et al., 2011; Ó Cofaigh et al., 2013a). There were more major ice streams originating from west Greenland than Baffin Island (Fig. 1) (Brouard and Lajeunesse, 2017; Jennings et al., 2017; Margold et al., 2018; Ó Cofaigh et al., 2013b; Simon et al., 2014). A wider shelf dissected by larger trough and fan systems suggests a dominant delivery of sediments into Baffin Bay via major west Greenland ice streams, which would have had a longer ice stream flow path with greater opportunity for erosion (Ó Cofaigh et al., 2013a; Simon et al., 2014).

The BBDC events are noted to occur during both warmer interstadial and cooler stadial conditions, suggesting that the North Atlantic climate may not be the dominant driver of deglaciation of the LIS, GIS and IIS (Jackson et al., 2017). Laurentide Ice Sheet discharge events have been linked to mainly stadial periods, whereas sediment delivery from the GIS has been linked to retreat driven by warmer atmospheric and oceanic temperatures within Baffin Bay (Jennings et al., 2011; Simon et al., 2014). The updated timings for BBDC1 and BBDC0 (Fig. 3) both now correspond to the relatively warmer periods of the Bølling-Allerød interstadial period and potentially MWP1A (Deschamps et al., 2012; Rasmussen et al., 2006) and the warming and recovery from the Younger Dryas as seen in the NGRIP and GISP2 ice core data (Fig. 6) (Rasmussen et al., 2006). The presence of an ice shelf blocking southern Baffin Bay has been debated in the past, but recent studies suggest this is unlikely during this time period (Jennings et al., 2018; Marcott et al., 2011; and references therein). A recent study, however, has shown evidence of a large ice shelf instead spanning the north of Baffin Bay during the LGM and subsequent deglaciation (Couette et al., 2022). It is thought the ice shelf started to develop and advance ~26 to 24.7 cal ka BP, before its rapid collapse by ~14.2 cal ka BP (Couette et al., 2022). The collapse of the ice shelf resulted in the unbuttressing of ice streams in the north and north-eastern Baffin Island, as well as the Lancaster Sound ice stream. It thus accelerated their breakup and retreat, with increased delivery of carbonate material into Baffin Bay signifying the final collapse of the ice shelf (Couette et al., 2022). The timing of this breakup is coincident with the revised date of 14.1 cal ka BP from this study for the start of BBDC1, and so would appear to support the ice shelf theory. Although not as extensively studied, it is also possible that the proposed ice shelf covering northern Baffin Bay reached a similar extent across the width of the bay (which could therefore have reached ice streams of central west Greenland, with the likelihood of at least fringing ice shelves along the margin) and so could have been associated with ice streams from the GIS (Couette et al., 2022). Therefore the collapse of the ice shelf could also have unbutressed ice streams of the GIS, accelerating break up and contributing to the more radiogenic $^{187}Os/^{188}Os$. It is likely therefore that the Ca and radiogenic $^{187}Os/^{188}Os$ rich sediments of BBDC1 are linked to a northeren Baffin Bay ice shelf collapse and subsequent accelerated ice stream discharge (i.e. Lancaster Sound ice stream and central-west Greenland ice streams) during the Bølling-Allerød. The relative reduction in reduced Ca and $^{187}Os/^{188}Os$ (Fig. 6) proceeding BBDC1 may then represent the end of this ice shelf breakup. The Ca and radiogenic $^{187}Os/^{188}Os$ rich sediments of BBDC0 are then likely due to the subsequent warming and recovery from the Younger Dryas cold period causing increased iceberg discharge after the temporary re-advance or pause in ice stream retreat (e.g., Furze et al., 2018; Jackson et al., 2017; Jennings et al., 2017; Margold et al., 2018; Ó Cofaigh et al., 2013b). However, there is a-synchronicity of the Ca and $^{187}Os/^{188}Os$ levels as the $^{187}Os/^{188}Os$ signature decreases *c.* 300 years before the decrease in Ca, suggesting the delivery of radiogenic material from a West Greenland (and/or Baffin Island) source ceased or significantly decreased before the flux of carbonate material from northern Baffin Bay ice streams.

The radiogenic Os signature can be linked to a west Greenland source, however, a partial Baffin Island source cannot be definitively ruled out. Although smaller than west Greenland ice streams, a number of ice streams existed along the Baffin Island shelf and flowed into Baffin Bay including for example, Home Bay, Scott Inlet, Buchan Gulf and Merchants Bay (Briner et al., 2003; Brouard and Lajeunesse, 2017; Margold et al., 2018). A sediment provenance reconstruction using qXRD data with SedUnMix has suggested that short pulses of coarse Baffin Island sediment occur within BBDC layers (Simon et al., 2014). However, a recent study has shown that the northeast Baffin Island slope and Baffin Island shelf receives sediments delivered from the smaller Baffin Island ice streams, whereas sediment deposition in central Baffin Bay is supplied via larger ice streams from, for example, Lancaster Sound (Jenner et al., 2018).

7. Conclusions

In summary we applied a multi-proxy suite of analyses including $^{187}Os/^{188}Os$, Ca, REE, mixing model, leach experiments and a new radiocarbon calibration method to investigate the timing and provenance of sediment delivery during BBDC layers from a core in central Baffin Bay. The results show that radiogenic peaks in $^{187}Os/^{188}Os$ are highly coincident with BBDC1 and BBDC0 but are not sourced from the same carbonate rocks as the BBDC layers. High $^{187}Os/^{188}Os$ values and REE profiles point to a radiogenic, felsic sediment source. They must therefore originate from the Archean to Paleoproterozoic aged terranes of central-west Greenland and/or Baffin Island, but distinguishing between the two sources is difficult. The physiography of Baffin Bay and surrounding ice streams, and a previous study using $^{187}Os/^{188}Os$ around central-west Greenland (Rooney et al., 2016) indicate that central-west GIS ice streams were the more likely source of radiogenic material alongside the carbonate material in BBDC layers.

Additionally, we use a new, updated method for calibration of radiocarbon dates taken from marine polar latitudes, taking into account the difficulties of reservoir correction in these localities. Through this we can provide new age constraints for BBDC1 of 14.1–13.0 cal ka BP, and BBDC0 of 12.0–10.9 cal ka BP. Both BBDC layers are now contemporaneous with relatively warmer climates as BBDC1 is coincident with the Bølling-Allerød interstadial and BBDC0 is coincident with the warming and recovery from the Younger Dryas cold period. It is likely that the Ca and radiogenic $^{187}Os/^{188}Os$ rich sediments of BBDC1 are a response to break up of an ice shelf covering northern Baffin Bay and subsequent acceleration of ice streams and sediment flux from Lancaster Sound and the GIS. The Ca and radiogenic $^{187}Os/^{188}Os$ rich sediments of BBDC0 are most likely the result of the subsequent warming and recovery from the Younger Dryas cold period causing increased iceberg discharge and sediment delivery from ice streams on the shelf.

Author contributions

Conceptualisation: EO, DS, JL, Laboratory analysis/sample collection: EO, PK, JA, SS, CO, Supervision: DS, JL, Writing – original draft: EO, Writing – review and editing: EO, DS, JL, PK, JA, CO.

Funding

This study was part funded by a NERC IAPETUS DTP studentship NE/L002590/1 (EO) and from a Yorkshire Geological Society (YGS) research fund grant (EO). Core JR175-GC01 was collected during cruise JR175 of the *RRS James Clark Ross* in 2009 (funded by NERC grant NE/D001951/1).

Declaration of competing interest

The authors declare that they have no known competing financial interests or personal relationships that could have appeared to influence the work reported in this paper.

Data availability

All accompanying data relating to this study can be found in the supplementary materials Excel file

Acknowledgements

We thank Peter Codling for allowing us to use data collected during his MSc at Durham University including XRF, foraminifera, IRD, grain size and core photos and X-rays. We thank Chris Ottley, Geoffrey Nowell, Emily Unsworth, Antonia Hoffman Chris Longley and Neil Tunstall at Durham University for laboratory assistance. We would also like to thank Keith Dewing (Geological Survey of Canada) and Professor Elizabeth Turner (Laurentian University) for providing us the carbonate rock samples from Somerset and Devon Islands used in this study. We also thank the reviewers and editor for their constructive and detailed comments. Finally, we would like to thank Professor Tim Heaton (University of Leeds) for helpful discussion regarding the best way to approach creating an age-depth model using both a Holocene and glacial reservoir correction.

Appendix A. Supplementary data

Supplementary data to this article can be found online at https://doi.org/10.1016/j.quascirev.2023.108082.

References

Aksu, A.E., Piper, D.J.W., 1987. Late quaternary sedimentation in baffin bay. Can. J. Earth Sci. 24, 1833–1846. https://doi.org/10.1139/e87-174.

Aksu, A.E., Piper, D.J.W., 1979. Baffin Bay in the past 100,000 yr. Geology 7, 245–248. https://doi.org/10.1130/0091-7613(1979)7<245:BBITPY>2.0.CO;2.

Andrews, J.T., 2019. Baffin Bay/Nares Strait surface (seafloor) sediment mineralogy: further investigations and methods to elucidate spatial variations in provenance. Can. J. Earth Sci. 56, 814–828. https://doi.org/10.1139/cjes-2018-0207.

Andrews, J.T., 1987. Late quaternary marine sediment accumulation in fiord-shelf-deep-sea transects, baffin island to baffin bay. Quat. Sci. Rev. 6, 231–243.

Andrews, J.T., Bjork, A.A., Eberl, D.D., Jennings, A.E., Verplanck, E.P., 2015. Significant differences in late Quaternary bedrock erosion and transport: east versus West Greenland ~70°N - evidence from the mineralogy of offshore glacial marine sediments. J. Quat. Sci. 30, 452–463. https://doi.org/10.1002/jqs.2787.

Andrews, J.T., Eberl, D.D., 2011. Surface (sea floor) and near-surface (box cores) sediment mineralogy in Baffin Bay as a key to sediment provenance and ice sheet variations. Can. J. Earth Sci. 48, 1307–1328. https://doi.org/10.1139/e11-021.

Andrews, J.T., Gibb, O.T., Jennings, A.E., Simon, Q., 2014. Variations in the provenance of sediment from ice sheets surrounding baffin bay during MIS 2 and 3 and export to the labrador shelf sea: site HU2008029-0008 Davis Strait. J. Quat. Sci. 29, 3–13. https://doi.org/10.1002/jqs.2643.

Andrews, J.T., Jenner, K.A., Campbell, C., 2020. Linking marine core lithofacies and mineral and grain-size compositions on the baffin island margin: changes in provenance and transport. J. Sediment. Res. 90, 763–775. https://doi.org/10.2110/jsr.2020.50.

Andrews, J.T., Kirby, M.E., Aksu, A.E., Barber, D.C., Meese, D., 1998. Late quaternary detrital carbonate (DC-) layers in Baffin Bay marine sediments (67°-74°N): correlation with Heinrich events in the North Atlantic? Quat. Sci. Rev. 17, 1125–1137. https://doi.org/10.1016/S0277-3791(97)00064-4.

Andrews, J.T., Klein, A.J., Jenner, K.A., Jennings, A.E., Campbell, C., 2018. The variability of Baffin Bay seafloor sediment mineralogy: the identification of discrete glacial sediment sources and application to Late Quaternary downcore analysis. Can. J. Earth Sci. 55, 620–639. https://doi.org/10.1139/cjes-2017-0223.

Batchelor, C.L., Margold, M., Krapp, M., Murton, D.K., Dalton, A.S., Gibbard, P.L., Stokes, C.R., Murton, J.B., Manica, A., 2019. The configuration of Northern Hemisphere ice sheets through the Quaternary. Nat. Commun. 10, 1–10. https://doi.org/10.1038/s41467-019-11601-2.

Bhatia, M.R., Crook, K.A.W., 1986. Trace element characteristics of graywackes and tectonic setting discrimination of sedimentary basins. Contrib. Mineral. Petrol. 92, 181–193. https://doi.org/10.1007/BF00375292.

Blaauw, M., 2012. Out of tune: the dangers of aligning proxy archives. Quat. Sci. Rev. 36, 38–49. https://doi.org/10.1016/j.quascirev.2010.11.012.

Blaauw, M., Christen, J.A., 2011. Flexible paleoclimate age-depth models using an autoregressive gamma process. Bayesian Anal 6, 457–474. https://doi.org/10.1214/11-BA618.

Blott, S.J., Croft, D.J., Pye, K., Saye, S.E., Wilson, H.E., 2004. Particle size analysis by laser diffraction. Geol. Soc. London, Spec. Publ. 232, 63–73. https://doi.org/10.1144/GSL.SP.2004.232.01.08.

Blott, S.J., Pye, K., 2001. Gradistat: a grain size distribution and statistics package for the analysis of unconsolidated sediments. Earth Surf. Process. Landforms 26, 1237–1248. https://doi.org/10.1002/esp.261.

Briner, J.P., Miller, G.H., Davis, P.T., Bierman, P.R., Caffee, M., 2003. Last glacial maximum ice sheet dynamics in Arctic Canada inferred from young erratics perched on ancient tors. Quat. Sci. Rev. 22, 437–444. https://doi.org/10.1016/S0277-3791(03)00003-9.

Briner, J.P., Miller, G.H., Davis, P.T., Finkel, R.C., 2006. Cosmogenic radionuclides from fiord landscapes support differential erosion by overriding ice sheets. Bull. Geol. Soc. Am. 118, 406–420. https://doi.org/10.1130/B25716.1.

Brouard, E., Lajeunesse, P., 2017. Maximum extent and decay of the Laurentide ice sheet in western baffin bay during the last glacial episode. Sci. Rep. 7, 1–8. https://doi.org/10.1038/s41598-017-11010-9.

Burton, K.W., Gannoun, A., Parkinson, I.J., 2010. Climate driven glacial-interglacial variations in the osmium isotope composition of seawater recorded by planktic foraminifera. Earth Planet Sci. Lett. 295, 58–68. https://doi.org/10.1016/j.epsl.2010.03.026.

Clark, P.U., Dyke, A.S., Shakun, J.D., Carlson, A.E., Clark, J., Wohlfarth, B., Mitrovica, J.X., Hostetler, S.W., McCabe, A.M., 2009. The last glacial maximum. Science (80 325, 710–714. https://doi.org/10.1126/science.1172873.

Codling, P., 2017. Late Quaternary Ice Sheet Dynamics and Palaeoceanography in the Baffin Bay Region. Durham University.

Couette, P.O., Lajeunesse, P., Ghienne, J.F., Dorschel, B., Gebhardt, C., Hebbeln, D., Brouard, E., 2022. Evidence for an extensive ice shelf in northern baffin bay during the last glacial maximum. Commun. Earth Environ. 3, 1–12. https://doi.org/10.1038/s43247-022-00559-7.

Dalai, T.K., Ravizza, G., 2006. Evaluation of osmium isotopes and iridium as paleo-flux tracers in pelagic carbonates. Geochem. Cosmochim. Acta 70, 3928–3942. https://doi.org/10.1016/j.gca.2006.06.002.

Dalai, T.K., Ravizza, G.E., Peucker-Ehrenbrink, B., 2006. The Late Eocene 187Os/188Os excursion: chemostratigraphy, cosmic dust flux and the Early Oligocene glaciation. Earth Planet Sci. Lett. 241, 477–492. https://doi.org/10.1016/j.epsl.2005.11.035.

Dalai, T.K., Suzuki, K., Minagawa, M., Nozaki, Y., 2005. Variations in seawater osmium isotope composition since the last glacial maximum: a case study from the Japan Sea. Chem. Geol. 220, 303–314. https://doi.org/10.1016/j.chemgeo.2005.04.012.

Dalton, A.S., Margold, M., Stokes, C.R., Tarasov, L., Dyke, A.S., Adams, R.S., Allard, S., Arends, H.E., Atkinson, N., Attig, J.W., Barnett, P.J., Barnett, R.L., Batterson, M., Bernatchez, P., Borns, H.W., Breckenridge, A., Briner, J.P., Brouard, E., Campbell, J.E., Carlson, A.E., Clague, J.J., Curry, B.B., Daigneault, R.A., Dubé-Loubert, H., Easterbrook, D.J., Franzi, D.A., Friedrich, H.G., Funder, S., Gauthier, M.S., Gowan, A.S., Harris, K.L., Hétu, B., Hooyer, T.S., Jennings, C.E., Johnson, M.D., Kehew, A.E., Kelley, S.E., Kerr, D., King, E.L., Kjeldsen, K.K., Knaeble, A.R., Lajeunesse, P., Lakeman, T.R., Lamothe, M., Larson, P., Lavoie, M., Loope, H.M., Lowell, T.V., Lusardi, B.A., Manz, L., McMartin, I., Nixon, F.C., Occhietti, S., Parkhill, M.A., Piper, D.J.W., Pronk, A.G., Richard, P.J.H., Ridge, J.C., Ross, M., Roy, M., Seaman, A., Shaw, J., Stea, R.R., Teller, J.T., Thompson, W.B., Thorleifson, L.H., Utting, D.J., Veillette, J.J., Ward, B.C., Weddle, T.K., Wright, H.E., 2020. An updated radiocarbon-based ice margin chronology for the last deglaciation of the North American Ice Sheet Complex. Quat. Sci. Rev. 234. https://doi.org/10.1016/j.quascirev.2020.106223.

Dalton, A.S., Stokes, C.R., Batchelor, C.L., 2022. Evolution of the Laurentide and innuitian ice sheets prior to the last glacial maximum (115 ka to 25 ka). Earth Sci. Rev. 224, 103875. https://doi.org/10.1016/j.earscirev.2021.103875.

Deschamps, P., Durand, N., Bard, E., Hamelin, B., Camoin, G., Thomas, A.L., Henderson, G.M., Okuno, J., Yokoyama, Y., 2012. Ice-sheet collapse and sea-level rise at the Bølling warming 14,600 years ago. Nature 483, 559–564. https://doi.org/10.1038/nature10902.

Dyke, A.S., Andrews, J.T., Clark, P.U., England, J., Miller, G.H., Shaw, J., Veillette, J.J., 2002. The Laurentide and innuitian ice sheets during the last glacial maximum. Quat. Sci. Rev. 21, 9–31. https://doi.org/10.1016/S0277-3791(01)00095-6.

Eberl, D.D., 2003. User's guide to RockJock - a program for determining quantitative mineralogy from powder X-ray diffraction data. U.S. Geol. Surv. Open File Rep. 78. https://doi.org/10.3133/ofr200378, 2003.

England, J., Atkinson, N., Bednarski, J., Dyke, A.S., Hodgson, D.A., Ó Cofaigh, C., 2006. The Innuitian Ice Sheet: configuration, dynamics and chronology. Quat. Sci. Rev. 25, 689–703. https://doi.org/10.1016/j.quascirev.2005.08.007.

Feyling-Hanssen, R.W., 1964. Foraminifera in late quatenary deposits from oslofjord area. Norges Geol. Undersøkelse 225, 1–383.

Finlay, A.J., Selby, D., Gröcke, D.R., 2010. Tracking the Hirnantian glaciation using Os isotopes. Earth Planet Sci. Lett. 293, 339–348. https://doi.org/10.1016/j.epsl.2010.02.049.

Furze, M.F.A., Pieńkowski, A.J., McNeely, M.A., Bennett, R., Cage, A.G., 2018. Deglaciation and ice shelf development at the northeast margin of the Laurentide Ice Sheet during the Younger Dryas chronozone. Boreas 47, 271–296. https://doi.org/10.1111/bor.12265.

Gottschalk, J., Szidat, S., Michel, E., Mazaud, A., Salazar, G., Battaglia, M., Lippold, J., Jaccard, S.L., 2018. Radiocarbon measurements of small-size foraminiferal samples with the mini carbon dating system (MICADAS) at the University of bern: implications for paleoclimate reconstructions. Radiocarbon 60, 469–491. https://doi.org/10.1017/RDC.2018.3.

Gregersen, U., Knutz, P.C., Hopper, J.R., 2016. New geophysical and geological mapping of the eastern Baffin Bay region, offshore West Greenland. Geol. Surv. Den. Greenl. Bull. 35, 83–86. https://doi.org/10.34194/geusb.v35.4945.

Harrison, J.C., St-Onge, M.R., Petrov, O.V., Strelnikov, S.I., Lopatin, B.G., Wilson, F.H., Tella, S., Paul, D., Lynds, T., Shokalsky, S.P., Hults, C.K., Bergman, S., Jepsen, H.F., Solli, A., 2011. Geological Map of the Arctic. Geol. Surv. Canada Map 2159A.

Heaton, T.J., Bard, E., Bronk Ramsey, C., Butzin, M., Hatté, C., Hughen, K.A., Köhler, P., Reimer, P.J., 2023. A response to community questions on the MARINE20 radiocarbon age calibration curve: marine reservoir ages and the calibration of 14 C samples from the oceans. Radiocarbon 65, 247–273. https://doi.org/10.1017/RDC.2022.66.

Heaton, T.J., Butzin, M., Bard, E., Bronk Ramsey, C., Hughen, K.A., Köhler, P., Reimer, P.J., 2022. Marine radiocarbon calibration in polar regions: a simple approximate approach using Marine20. EarthArXiv. Submitt. to J. Radiocarb. Rev.

Heaton, T.J., Köhler, P., Butzin, M., Bard, E., Reimer, R.W., Austin, W.E.N., Bronk Ramsey, C., Grootes, P.M., Hughen, K.A., Kromer, B., Reimer, P.J., Adkins, J., Burke, A., Cook, M.S., Olsen, J., Skinner, L.C., 2020. Marine20 - the marine radiocarbon age calibration curve (0-55,000 cal BP). Radiocarbon 62, 779–820. https://doi.org/10.1017/RDC.2020.68.

Henriksen, N., Higgins, A.K., 2009. Descriptive text to geological map of Greenland, 1:500 000, dove Bugt, sheet 10. Geol. Surv. Denmark Greenl. Map Ser. 4, 1–32. https://doi.org/10.34194/geusm.v4.4581.

Hogan, K.A., Ó Cofaigh, C., Jennings, A.E., Dowdeswell, J.A., Hiemstra, J.F., 2016. Deglaciation of a major palaeo-ice stream in Disko Trough, west Greenland. Quat. Sci. Rev. 147, 5–26. https://doi.org/10.1016/j.quascirev.2016.01.018.

Hudson, B., Overeem, I., McGrath, D., Syvitski, J.P.M., Mikkelsen, A., Hasholt, B., 2014. MODIS observed increase in duration and spatial extent of sediment plumes in Greenland fjords. Cryosphere 8, 1161–1176. https://doi.org/10.5194/tc-8-1161-2014.

Jackson, R., Carlson, A.E., Hillaire-Marcel, C., Wacker, L., Vogt, C., Kucera, M., 2017. Asynchronous instability of the North American-Arctic and Greenland ice sheets during the last deglaciation. Quat. Sci. Rev. 164, 140–153. https://doi.org/10.1016/j.quascirev.2017.03.020.

Jenner, K.A., Campbell, D.C., Piper, D.J.W., 2018. Along-slope variations in sediment lithofacies and depositional processes since the Last Glacial Maximum on the northeast Baffin margin, Canada. Mar. Geol. 405, 92–107. https://doi.org/10.1016/j.margeo.2018.07.012.

Jennings, A.E., Andrews, J.T., Ó Cofaigh, C., Onge, G.S., Sheldon, C., Belt, S.T., Cabedo-Sanz, P., Hillaire-Marcel, C., 2017. Ocean forcing of Ice Sheet retreat in central west Greenland from LGM to the early Holocene. Earth Planet Sci. Lett. 472, 1–13. https://doi.org/10.1016/j.epsl.2017.05.007.

Jennings, A.E., Andrews, J.T., Ó Cofaigh, C., St-Onge, G., Belt, S.T., Cabedo-Sanz, P., Pearce, C., Hillaire-Marcel, C., Calvin Campbell, D., 2018. Baffin Bay paleo-environments in the LGM and HS1: resolving the ice-shelf question. Mar. Geol. 402, 5–16. https://doi.org/10.1016/j.margeo.2017.09.002.

Jennings, A.E., Sheldon, C., Cronin, T.M., Francus, P., Stoner, J., Andrews, J., 2011. The holocene history of nares strait. Oceanography 24, 26–41. https://doi.org/10.5670/oceanog.2011.52.

Jennings, A.E., Walton, M.E., Ó Cofaigh, C., Kilfeather, A., Andrews, J.T., Ortiz, J.D., De Vernal, A., Dowdeswell, J.A., 2014. Paleoenvironments during younger dryas-early holocene retreat of the Greenland ice sheet from outer Disko Trough, central west Greenland. J. Quat. Sci. 29, 27–40. https://doi.org/10.1002/jqs.2652.

Kelleher, R., Jennings, A., Andrews, J., Brooks, N.K.S., Marchitto, T., Feng, S., Woelders, L., Normandeau, A., Jenner, K., Bennett, R., Brookins, S., 2022. Late Glacial Retreat of the Lancaster Sound Ice Stream and Early Holocene Onset of Arctic/Atlantic Throughflow in the Arctic Island Channels, Arctic, Antarctic, and Alpine Research. Taylor & Francis. https://doi.org/10.1080/15230430.2022.2110689.

Kirillova, V., 2017. Radiogenic Isotopes on Marine Sediments from the Baffin Bay: Implications for the Sediment Supply during the Last Deglaciation. Bremen University.

Knutz, P.C., Gregersen, U., Harrison, C., Brent, T.A., Hopper, J.R., Nøhr-Hansen, H., 2022. Baffin bay composite tectono-sedimentary element. Geol. Soc. London, Mem. 57. https://doi.org/10.1144/M57-2016-7.

Knutz, P.C., Newton, A.M.W., Hopper, J.R., Huuse, M., Gregersen, U., Sheldon, E., Dybkjær, K., 2019. Eleven phases of Greenland Ice Sheet shelf-edge advance over the past 2.7 million years. Nat. Geosci. 12, 361–368. https://doi.org/10.1038/s41561-019-0340-8.

Knutz, P.C., Sicre, M.A., Ebbesen, H., Christiansen, S., Kuijpers, A., 2011. Multiple-stage deglacial retreat of the southern Greenland Ice Sheet linked with Irminger Current warm water transport. Paleoceanography 26, 1–18. https://doi.org/10.1029/2010PA002053.

Li, G., Piper, D.J.W., Calvin Campbell, D., 2011. The quaternary lancaster Sound trough-mouth fan, NW baffin bay. J. Quat. Sci. 26, 511–522. https://doi.org/10.1002/jqs.1479.

Lloyd, J.M., 2006. Modern distribution of benthic foraminifera from Disko Bugt, west Greenland. J. Foraminifer. Res. 36, 315–331. https://doi.org/10.2113/gsjfr.36.4.315.

Luguet, A., Nowell, G.M., Pearson, D.G., 2008. 184Os/188Os and 186Os/188Os measurements by Negative Thermal Ionisation Mass Spectrometry (N-TIMS): effects of interfering element and mass fractionation corrections on data accuracy and precision. Chem. Geol. 248, 342–362. https://doi.org/10.1016/j.chemgeo.2007.10.013.

Marcott, S.A., Clark, P.U., Padman, L., Klinkhammer, G.P., Springer, S.R., Liu, Z., Otto-Bliesner, B.L., Carlson, A.E., Ungerer, A., Padman, J., He, F., Cheng, J., Schmittner, A., 2011. Ice-shelf collapse from subsurface warming as a trigger for Heinrich events. Proc. Natl. Acad. Sci. U.S.A. 108, 13415–13419. https://doi.org/10.1073/pnas.1104772108.

Margold, M., Stokes, C.R., Clark, C.D., 2018. Reconciling records of ice streaming and ice margin retreat to produce a palaeogeographic reconstruction of the deglaciation of the Laurentide Ice Sheet. Quat. Sci. Rev. 189, 1–30. https://doi.org/10.1016/j.quascirev.2018.03.013.

McCarty, D.K., 2002. Quantitative mineral analysis of clay-bearing mixtures: the "Reynolds Cup" contest. Int. Union Crystallogr. 27, 12–16.

McLennan, S.M., 2001. Relationships between the trace element composition of sedimentary rocks and upper continental crust. G-cubed 2, n. https://doi.org/10.1029/2000GC000109.

Missiaen, L., Wacker, L., Lougheed, B.C., Skinner, L., Hajdas, I., Nouet, J., Pichat, S., Waelbroeck, C., 2020. Radiocarbon dating of small-sized foraminifer samples: insights into marine sediment mixing. Radiocarbon 62, 313–333. https://

doi.org/10.1017/RDC.2020.13.
Ó Cofaigh, C., Andrews, J.T., Jennings, A.E., Dowdeswell, J.A., Hogan, K.A., Kilfeather, A.A., Sheldon, C., 2013a. Glacimarine lithofacies, provenance and depositional processes on a West Greenland trough-mouth fan. J. Quat. Sci. 28, 13–26. https://doi.org/10.1002/jqs.2569.
Ó Cofaigh, C., Dowdeswell, J.A., Jennings, A.E., Hogan, K.A., Kilfeather, A., Hiemstra, J.F., Noormets, R., Evans, J., McCarthy, D.J., Andrews, J.T., Lloyd, J.M., Moros, M., 2013b. An extensive and dynamic ice sheet on the West Greenland shelf during the last glacial cycle. Geology 41, 219–222. https://doi.org/10.1130/G33759.1.
Ó Cofaigh, C., Hogan, K.A., Jennings, A.E., Callard, S.L., Dowdeswell, J.A., Noormets, R., Evans, J., 2018. The role of meltwater in high-latitude trough-mouth fan development: the Disko Trough-Mouth Fan, West Greenland. Mar. Geol. 402, 17–32. https://doi.org/10.1016/j.margeo.2018.02.001.
Ó Cofaigh, C., Weilbach, K., Lloyd, J.M., Benetti, S., Callard, S.L., Purcell, C., Chiverrell, R.C., Dunlop, P., Saher, M., Livingstone, S.J., Van Landeghem, K.J.J., Moreton, S.G., Clark, C.D., Fabel, D., 2019. Early deglaciation of the British-Irish Ice Sheet on the Atlantic shelf northwest of Ireland driven by glacioisostatic depression and high relative sea level. Quat. Sci. Rev. 208, 76–96. https://doi.org/10.1016/j.quascirev.2018.12.022.
Oxburgh, R., 1998. Variations in the osmium isotope composition of seawater over the past 200 000 years. Earth Planet Sci. Lett. 159, 183–191. https://doi.org/10.1016/S0012-821X(98)00057-0.
Oxburgh, R., Pierson-Wickmann, A.-C., Reisberg, L., Hemming, S., 2007. Climate-correlated variations in seawater 187Os/188Os over the past 200,000 yr: evidence from the cariaco basin, Venezuela. Earth Planet Sci. Lett. 263, 246–258. https://doi.org/10.1016/j.epsl.2007.08.033.
Paquay, F.S., Goderis, S., Ravizza, G., Vanhaeck, F., Boyd, M., Surovell, T.A., Holliday, V.T., Haynes, C.V., Claeys, P., 2009. Absence of geochemical evidence for an impact event at the Bølling–Allerød/Younger Dryas transition. Proc. Natl. Acad. Sci. USA 106, 21505–21510. https://doi.org/10.1073/pnas.0908874106.
Paquay, F.S., Ravizza, G., 2012. Heterogeneous seawater 187Os/188Os during the late Pleistocene glaciations. Earth Planet Sci. Lett. 349 (350), 126–138. https://doi.org/10.1016/j.epsl.2012.06.051.
Pettijohn, F.J., Potter, P.E., Siever, R., 1987. Sand and Sandstone. Springer, New York, New York, NY. https://doi.org/10.1007/978-1-4612-1066-5.
Peucker-Ehrenbrink, B., Blum, J.D., 1998. Re-Os isotope systematics and weathering of Precambrian crustal rocks: implications for the marine osmium isotope record. Geochem. Cosmochim. Acta 62, 3193–3203. https://doi.org/10.1016/S0016-7037(98)00227-0.
Peucker-Ehrenbrink, B., Jahn, 2001. The upper continental crust. G-cubed 2, 1–22.
Peucker-Ehrenbrink, B., Ravizza, G., 2000. The marine osmium isotope record. Terra. Nova 12, 205–219. https://doi.org/10.1046/j.1365-3121.2000.00295.x.
Rasmussen, S.O., Andersen, K.K., Svensson, A.M., Steffensen, J.P., Vinther, B.M., Clausen, H.B., Siggaard-Andersen, M.L., Johnsen, S.J., Larsen, L.B., Dahl-Jensen, D., Bigler, M., Röthlisberger, R., Fischer, H., Goto-Azuma, K., Hansson, M.E., Ruth, U., 2006. A new Greenland ice core chronology for the last glacial termination. J. Geophys. Res. Atmos. 111. https://doi.org/10.1029/2005JD006079.
Rasmussen, S.O., Bigler, M., Blockley, S.P., Blunier, T., Buchardt, S.L., Clausen, H.B., Cvijanovic, I., Dahl-Jensen, D., Johnsen, S.J., Fischer, H., Gkinis, V., Guillevic, M., Hoek, W.Z., Lowe, J.J., Pedro, J.B., Popp, T., Seierstad, I.K., Steffensen, J.P., Svensson, A.M., Vallelonga, P., Vinther, B.M., Walker, M.J.C., Wheatley, J.J., Winstrup, M., 2014. A stratigraphic framework for abrupt climatic changes during the Last Glacial period based on three synchronized Greenland ice-core records: refining and extending the INTIMATE event stratigraphy. Quat. Sci. Rev. 106, 14–28. https://doi.org/10.1016/j.quascirev.2014.09.007.
Reimer, P.J., Austin, W.E.N., Bard, E., Bayliss, A., Blackwell, P.G., Bronk Ramsey, C., Butzin, M., Cheng, H., Edwards, R.L., Friedrich, M., Grootes, P.M., Guilderson, T.P., Hajdas, I., Heaton, T.J., Hogg, A.G., Hughen, K.A., Kromer, B., Manning, S.W., Muscheler, R., Palmer, J.G., Pearson, C., Van Der Plicht, J., Reimer, R.W., Richards, D.A., Scott, E.M., Southon, J.R., Turney, C.S.M., Wacker, L., Adolphi, F., Büntgen, U., Capano, M., Fahrni, S.M., Fogtmann-Schulz, A., Friedrich, R., Köhler, P., Kudsk, S., Miyake, F., Olsen, J., Reinig, F., Sakamoto, M., Sookdeo, A., Talamo, S., 2020. The IntCal20 northern hemisphere radiocarbon age calibration curve (0-55 cal kBP). Radiocarbon 62, 725–757. https://doi.org/10.1017/RDC.2020.41.
Reimer, P.J., Edouard Bard, B., Alex Bayliss, B., Warren Beck, B.J., Paul Blackwell, B.G., Christopher Bronk Ramsey, B., 2013. Intcal13 and Marine13 radiocarbon age calibration curves 0–50,000 Years cal bp. Radiocarbon 55, 1869. https://doi.org/10.1017/S0033822200048864. –1887.
Rooney, A.D., Macdonald, F.A., Strauss, J.V., Dudás, F.Ö., Hallmann, C., Selby, D., 2014. Re-Os geochronology and coupled Os-Sr isotope constraints on the Sturtian snowball Earth. Proc. Natl. Acad. Sci. U.S.A. 111, 51–56. https://doi.org/10.1073/pnas.1317266110.
Rooney, A.D., Selby, D., Lloyd, J.M., Roberts, D.H., Lückge, A., Sageman, B.B., Prouty, N.G., 2016. Tracking millennial-scale Holocene glacial advance and retreat using osmium isotopes: insights from the Greenland ice sheet. Quat. Sci. Rev. 138, 49–61. https://doi.org/10.1016/j.quascirev.2016.02.021.
Scott, D.B., Medioli, F.S., Schafer, C.T., 2001. Monitoring in Coastal Environments Using Foraminifera and Thecamoebian Indicators. Cambridge University Press. https://doi.org/10.1017/CBO9780511546020.
Seierstad, I.K., Abbott, P.M., Bigler, M., Blunier, T., Bourne, A.J., Brook, E., Buchardt, S.L., Buizert, C., Clausen, H.B., Cook, E., Dahl-Jensen, D., Davies, S.M., Guillevic, M., Johnsen, S.J., Pedersen, D.S., Popp, T.J., Rasmussen, S.O., Severinghaus, J.P., Svensson, A., Vinther, B.M., 2014. Consistently dated records from the Greenland GRIP, GISP2 and NGRIP ice cores for the past 104ka reveal regional millennial-scale δ18O gradients with possible Heinrich event imprint. Quat. Sci. Rev. 106, 29–46. https://doi.org/10.1016/j.quascirev.2014.10.032.
Selby, D., Creaser, R.A., 2003. Re-Os geochronology of organic rich sediments: an evaluation of organic matter analysis methods. Chem. Geol. 200, 225–240. https://doi.org/10.1016/S0009-2541(03)00199-2.
Selby, D., Creaser, R.A., Nesbitt, B.E., 1999. Major and trace element compositions and Sr-Nd-Pb systematics of crystalline rocks from the Dawson Range, Yukon, Canada. Can. J. Earth Sci. 36, 1463–1481. https://doi.org/10.1139/e99-058.
Sheldon, C., Jennings, A., Andrews, J.T., Ó Cofaigh, C., Hogan, K., Dowdeswell, J.A., Seidenkrantz, M.S., 2016. Ice stream retreat following the LGM and onset of the west Greenland current in Uummannaq Trough, west Greenland. Quat. Sci. Rev. 147, 27–46. https://doi.org/10.1016/j.quascirev.2016.01.019.
Shirey, S.B., Walker, R.J., 1998. THE R <scp>e</scp> -O <scp>s</scp> ISOTOPE SYSTEM IN COSMOCHEMISTRY AND HIGH-TEMPERATURE GEOCHEMISTRY. Annu. Rev. Earth Planet Sci. 26, 423–500. https://doi.org/10.1146/annurev.earth.26.1.423.
Simon, Q., Hillaire-Marcel, C., St-Onge, G., Andrews, J.T., 2014. North-eastern Laurentide, western Greenland and southern Innuitian ice stream dynamics during the last glacial cycle. J. Quat. Sci. 29, 14–26. https://doi.org/10.1002/jqs.2648.
Simon, Q., St-Onge, G., Hillaire-Marcel, C., 2012. Late Quaternary chronostratigraphic framework of deep Baffin Bay glaciomarine sediments from high-resolution paleomagnetic data. G-cubed 13, 1–24. https://doi.org/10.1029/2012GC004272.
Sproson, A.D., Pogge von Strandmann, P.A.E., Selby, D., Jarochowska, E., Frýda, J., Hladil, J., Loydell, D.K., Slavík, L., Calner, M., Maier, G., Munnecke, A., Lenton, T.M., 2022. Osmium and lithium isotope evidence for weathering feedbacks linked to orbitally paced organic carbon burial and Silurian glaciations. Earth Planet Sci. Lett. 577. https://doi.org/10.1016/j.epsl.2021.117260.
St-Onge, M.R., Van Gool, J.A.M., Garde, A.A., Scott, D.J., 2009. Correlation of Archaean and Palaeoproterozoic units between northeastern Canada and western Greenland: constraining the pre-collisional upper late accretionary history of the Trans-Hudson orogen. Geol. Soc. Spec. Publ. 318, 193–235. https://doi.org/10.1144/SP318.7.
Stuiver, M., Grootes, P.M., 2000. GISP2 oxygen isotope ratios. Quat. Res. 53, 277–284. https://doi.org/10.1006/qres.2000.2127.
Stuiver, M., Reimer, P.J., Reimer, R.W., 2020. CALIB 7.1 [WWW program].
Szidat, S., Salazar, G.A., Vogel, E., Battaglia, M., Wacker, L., Synal, H.-A., Türler, A., 2014. 14 C analysis and sample preparation at the new bern laboratory for the analysis of radiocarbon with AMS (LARA). Radiocarbon 56, 561–566. https://doi.org/10.2458/56.17457.
Tang, C.C.L., Ross, C.K., Yao, T., Petrie, B., DeTracey, B.M., Dunlap, E., 2004. The circulation, water masses and sea-ice of Baffin Bay. Prog. Oceanogr. 63, 183–228. https://doi.org/10.1016/j.pocean.2004.09.005.
Taylor, S.R., McLennan, S.M., 1985. The Continental Crust: its Composition and Evolution. Blackwell Scientific Publications.
van der Ploeg, R., Selby, D., Cramwinckel, M.J., Li, Y., Bohaty, S.M., Middelburg, J.J., Sluijs, A., 2018. Middle Eocene greenhouse warming facilitated by diminished weathering feedback. Nat. Commun. 9, 2877. https://doi.org/10.1038/s41467-018-05104-9.
Williams, G.A., Turekian, K.K., 2004. The glacial–interglacial variation of seawater osmium isotopes as recorded in Santa Barbara Basin. Earth Planet Sci. Lett. 228, 379–389. https://doi.org/10.1016/j.epsl.2004.10.004.